

 Open access • Journal Article • DOI:10.1021/MA100713H

## Homogeneous Dispersion of Magnetic Nanoparticles Aggregates in a PS Nanocomposite: Highly Reproducible Hierarchical Structure Tuned by the Nanoparticles' Size — [Source link](#)

[Anne-Sophie Robbes](#), [Jacques Jestin](#), [Florian Meneau](#), [Florent Dalmas](#) ...+4 more authors

**Institutions:** [Centre national de la recherche scientifique](#), [ParisTech](#)

**Published on:** 01 Jun 2010 - [Macromolecules](#) (American Chemical Society)

**Topics:** [Magnetic nanoparticles](#), [Nanoparticle](#) and [Nanocomposite](#)

Related papers:

- [Well-Dispersed Fractal Aggregates as Filler in Polymer–Silica Nanocomposites: Long-Range Effects in Rheology](#)
- [Graphene/Polymer Nanocomposites](#)
- [Molecular Composites Comprising TiO<sub>2</sub> and Their Optical Properties](#)
- ["Wet-to-Dry" Conformational Transition of Polymer Layers Grafted to Nanoparticles in Nanocomposite](#)
- [Polymer-Grafted-Nanoparticles Nanocomposites: Dispersion, Grafted Chain Conformation, and Rheological Behavior](#)

Share this paper:    

View more about this paper here: <https://typeset.io/papers/homogeneous-dispersion-of-magnetic-nanoparticles-aggregates-4xdzldypu9>



**HAL**  
open science

# Homogeneous Dispersion of Magnetic Nanoparticles Aggregates in a PS Nanocomposite: Highly Reproducible Hierarchical Structure Tuned by the Nanoparticles' Size

Anne-Sophie Robbes, Jacques Jestin, Olivier Sandre, Florian Meneau, Florent Dalmas, Javier Perez, François Boué, Fabrice Cousin

► **To cite this version:**

Anne-Sophie Robbes, Jacques Jestin, Olivier Sandre, Florian Meneau, Florent Dalmas, et al.. Homogeneous Dispersion of Magnetic Nanoparticles Aggregates in a PS Nanocomposite: Highly Reproducible Hierarchical Structure Tuned by the Nanoparticles' Size. *Macromolecules*, American Chemical Society, 2010, 43 (13), pp.5785-5796. 10.1021/ma100713h . hal-00533476

**HAL Id: hal-00533476**

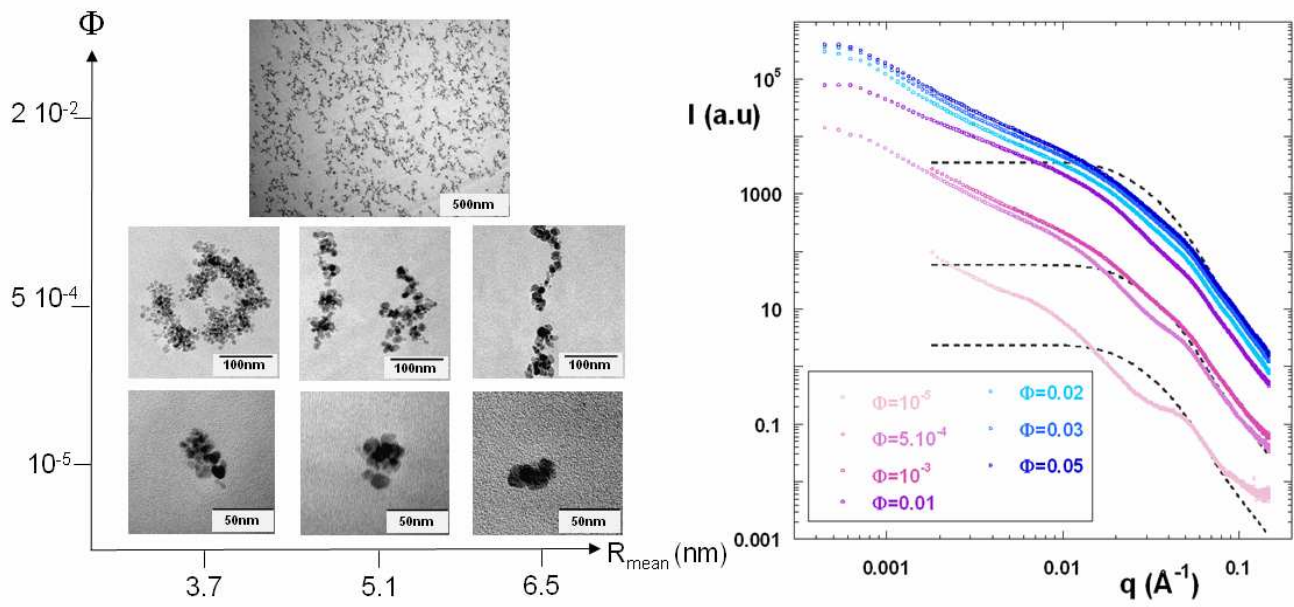
**<https://hal.archives-ouvertes.fr/hal-00533476>**

Submitted on 25 May 2019

**HAL** is a multi-disciplinary open access archive for the deposit and dissemination of scientific research documents, whether they are published or not. The documents may come from teaching and research institutions in France or abroad, or from public or private research centers.

L'archive ouverte pluridisciplinaire **HAL**, est destinée au dépôt et à la diffusion de documents scientifiques de niveau recherche, publiés ou non, émanant des établissements d'enseignement et de recherche français ou étrangers, des laboratoires publics ou privés.

Figure TOC



1  
2  
3  
4  
5  
6  
7  
8  
9  
10  
11  
12  
13  
14  
15  
16  
17  
18  
19  
20  
21  
22  
23  
24  
25  
26  
27  
28  
29  
30  
31  
32  
33  
34  
35  
36  
37  
38  
39  
40  
41  
42  
43  
44  
45  
46  
47  
48  
49  
50  
51  
52  
53  
54  
55  
56  
57  
58  
59  
60

# Homogeneous Dispersion of Magnetic Nanoparticles Aggregates in a PS Nanocomposite: Highly Reproducible Hierarchical Structure tuned by the Nanoparticles Size.

*Anne-Sophie Robbes<sup>1,2</sup>, Jacques Jestin<sup>1</sup>, Florian Meneau<sup>2</sup>, Florent Dalmas<sup>3</sup>, Olivier Sandre<sup>4</sup>, Javier  
Perez<sup>2</sup>, François Boué<sup>1</sup>, Fabrice Cousin<sup>1,\*</sup>*

<sup>1</sup>Laboratoire Léon Brillouin, CEA Saclay 91191 Gif sur Yvette, Cedex France

<sup>2</sup>Synchrotron SOLEIL, L'Orme des Merisiers, PO Box 48, Saint-Aubin, 91192 Gif sur Yvette, France

<sup>3</sup>Institut de Chimie et des Matériaux Paris-Est, CNRS UMR 7182, 2-8 rue Henri Dunant 94320 Thiais,  
France

<sup>4</sup>Laboratoire Physicochimie des Electrolytes, Colloïdes et Sciences Analytiques, UMR CNRS-UPMC-  
Univ Paris 6-ESPCI-Paris Tech 7195, 4 place Jussieu, case 51, 75005 Paris, France

**RECEIVED DATE (to be automatically inserted after your manuscript is accepted if required  
according to the journal that you are submitting your paper to)**

\* Corresponding author: [fabrice.cousin@cea.fr](mailto:fabrice.cousin@cea.fr)

## ABSTRACT

1  
2  
3  
4 We present here the synthesis and structural characterization of new nanocomposites made of spherical  
5  
6 magnetic nanoparticles of maghemite ( $\gamma\text{-Fe}_2\text{O}_3$ ) dispersed in a polystyrene (PS) matrix. The  $\gamma\text{-Fe}_2\text{O}_3$   
7  
8 nanoparticles, synthesized in aqueous media, were first gently transferred by dialysis in  
9  
10 dimethylacetamide (DMAc), a polar solvent which is a good solvent for PS. Electrostatic repulsions  
11  
12 enable to keep colloidal stability in DMAc. The nanocomposites were then processed by a controlled  
13  
14 evaporation of DMAc of binary mixtures of  $\gamma\text{-Fe}_2\text{O}_3$  nanoparticles and PS chains. The size of the  
15  
16 nanoparticles ranges from 3.5 to 6.5 nm and can be changed without any modification of the  
17  
18 nanoparticles' surface. The structural organization of the nanoparticles inside the polymer was  
19  
20 determined as a function of the nanoparticles' size. It was performed by combining very high resolution  
21  
22 SAXS measurements which permit to decrease the nanoparticles content down to very low values  
23  
24 ( $\Phi_{\text{mag}} \sim 10^{-5}$ ) and TEM microscopy. Whatever the size, the nanoparticles are organized with a  
25  
26 hierarchical structure that shows that their aggregation has been driven by a two-step process. At low  
27  
28 spatial scale, dense primary aggregates composed of some tens of nanoparticles are formed whatever  
29  
30  $\Phi_{\text{mag}}$ , resulting from the first aggregation step. For  $\Phi_{\text{mag}} > 10^{-4}$ , these primary aggregates underwent a  
31  
32 second aggregation step and are organized at larger scale in fractal aggregates of finite size of  $\sim 200\text{nm}$   
33  
34 of radius, with a dimension of 1.7. The size of the dense primary aggregates is almost constant when  
35  
36 changing the nanoparticles radius, i.e the mean aggregation number of primary aggregates decreases  
37  
38 with an increase of the radius.  
39  
40  
41  
42  
43  
44  
45  
46  
47  
48  
49  
50  
51  
52  
53  
54  
55  
56  
57  
58  
59  
60

## I Introduction

1  
2  
3  
4  
5 The mechanical properties of a polymeric film can be improved by the inclusion of hard particles inside  
6  
7 the matrix. In the last two decades, a specific attention has been focused on the reduction of the size of  
8  
9 the particles down to the nanometer range to increase the specific surface between the particles and the  
10  
11 polymer in order to improve both the reinforcement and the deformability of the resulting materials [1].  
12  
13 From an applicative point of view, the refined understanding of the mechanisms which govern the  
14  
15 properties of the filled-polymer system is of great interest in order to design new materials with  
16  
17 dedicated and controlled mechanical properties [2]. From a fundamental point of view, one still open  
18  
19 question is to correlate the structural and dynamical properties of the components of the system at the  
20  
21 microscopic level, i.e. the local structure of the filler and the polymer chain conformation, to the  
22  
23 macroscopic response of the material like the elastic modulus. It is now commonly admitted that both  
24  
25 the filler structure and chains dynamics contribute to the mechanisms of reinforcement. The contribution  
26  
27 of the filler network comes from possible reorganizations under stretching (displacement/rotation,  
28  
29 association/dissociation, and reorganization/breaking). It has been extensively studied from simple  
30  
31 hydrodynamic models [3] to percolation effects at large filler content [4-7] in the linear, but also in the  
32  
33 non linear regime with filler network breakdown and non affinity reorganizations [8]. The contribution  
34  
35 of the chains, either before deformation or under stretching, has also been studied by simulations [9] and  
36  
37 by experimental approaches [10, 11]. The emerging idea [12] to explain its influence on the  
38  
39 reinforcement effects is the existence of a fraction of chains under a “glassy” state which will contribute  
40  
41 to the elastic modulus as a rigid phase of the system. However, up to now, the direct measurement of  
42  
43 this glassy fraction is still under discussions [13] as both contributions, filler and chains, can be  
44  
45 correlated or not under deformation. As a consequence, it is difficult to separate their relative influence  
46  
47 on the final properties of the materials at the macroscopic scale. Different strategies have been recently  
48  
49 developed to elucidate these mechanisms by decoupling the contributions. Two main strategies are  
50  
51 explored: modifying the interactions without changing the filler structure, or changing the polymer-filler  
52  
53  
54  
55  
56  
57  
58  
59  
60

1 interactions without modifying the filler organization. The first method can be achieved by grafting the  
2 filler by the same polymeric chains as the ones of the matrix [14, 15]. It is attractive but implies to  
3 develop specific chemistry processes for the grafting of the filler. The second method, that can be  
4 achieved by a simpler processing route like simple mixing of components, offers nice perspectives for  
5 the design of model systems. Following this idea, some examples can be found using anisotropic or  
6 fractal fillers [16, 4] or changing the electrostatic interactions [17]. However, whatever the strategy used,  
7 changing the filler morphology at the local scale without changing organization at the large scale inside  
8 the polymer matrix by a simple tuning parameter (which is usually the particle content), is difficult  
9 because the filler-filler interactions usually depend of the filler concentration.

10 In the present paper, we present a new model system of filler-polymer nanocomposite that really enables  
11 to change the polymer-filler interactions without modifying the filler organization at large scale. It is  
12 made of polystyrene (PS) matrix reinforced by spherical magnetic nanoparticles of maghemite ( $\gamma$ -  
13  $\text{Fe}_2\text{O}_3$ ). Its specificity comes from the fact that different batches of nanoparticles with various mean radii  
14 ranging from 3.5 to 6.5 nm can be obtained starting from a single batch of nanoparticles after using a  
15 specific size-sorting process [18] based on colloidal gas-liquid transitions [19]. We thus dispose of a  
16 system for which the particle size can be finely tuned without making any surface modification. It  
17 provides us a new key parameter to manage the filler structure inside the polymer matrix. Such similar  
18 tuning of the particle size in nanocomposites is indeed rather difficult for other mineral particles, like  
19 silica for example, as it implies to synthesis each particles size separately, which results in surface  
20 modifications that can induce changes in polymer-filler interactions.

21 The use of magnetic nanoparticles has also a great potential interest for the improvement of the  
22 properties of polymeric systems in further studies. It has been demonstrated in the literature that it is  
23 possible to take advantage from the magnetic aspect of nanoparticles to design either magneto-  
24 stimuable crosslinked gels [20, 21] or to create controlled anisotropic structures in nanocomposites  
25 using a magnetic field during casting [22].

1 The paper is organized as follow: first we present the analysis of the nanoparticles in solution and  
2 especially the transfer from water to an organic solvent, dimethylacetamide, while keeping the colloidal  
3 stability using a dialysis process. Second, we have adapted the film processing developed by Jouault et  
4 al. [5] for silica fillers to our system in order to form homogeneous nanocomposites. Finally, the  
5 structure of the particles inside the polymer matrix is analyzed with a refined combination of high  
6 resolution SAXS measurements at the nanometer scale, which permit to cover a large range of particles  
7 volume fraction (from  $10^{-5}$  to  $5.10^{-2}$ ), with TEM microscopy which enable to validate the structure in the  
8 real space and the homogeneity at larger scale. The filler structure is then discussed as a function of the  
9 filler content and as a function of the tunable parameter, i.e. the native nanoparticles' size.  
10  
11  
12  
13  
14  
15  
16  
17  
18  
19  
20  
21  
22  
23

## 24 **II Materials and Methods**

### 25 *II.1 Synthesis of magnetic $\gamma$ -Fe<sub>2</sub>O<sub>3</sub> nanoparticles in aqueous solution*

26  
27  
28  
29  
30  
31 The maghemite ( $\gamma$ -Fe<sub>2</sub>O<sub>3</sub>) nanoparticles were chemically synthesized in water by coprecipitation in an  
32 aqueous ammonia solution of FeCl<sub>2</sub> and FeCl<sub>3</sub> salts. As a result we obtain colloidal magnetite which is  
33 fully oxidized to maghemite by Fe(NO<sub>3</sub>)<sub>3</sub> in acidic medium [23]. The experimental conditions have been  
34 chosen in order to prepare particles with an average radius of the order of 40 Å. They have a roughly  
35 spherical shape. A size-sorting process based on colloidal gas-liquid transitions allowed then to split up  
36 the population of nanoparticles according to their diameter [18]. 4 batches of nanoparticles, with  
37 different sizes, have been obtained by such fractionation of the initial suspension. The size of the  
38 nanoparticles of the different batches and their volume fraction of magnetic nanoparticles  $\Phi_{\text{mag}}$  were  
39 obtained by magnetization measurements performed with a home-made vibrating magnetometer device.  
40  
41  
42  
43  
44  
45  
46  
47  
48  
49  
50  
51  
52  
53  
54  
55  
56  
57  
58  
59  
60  
The principle of the determination of the distribution of the radii from the magnetization curve [24] is  
recalled in supporting Information. The sizes were also measured by SAXS (see table 1 in part III).

At the end of the synthesis, the positively charged naked nanoparticles were electrostatically stabilized  
at pH ~ 2 by HNO<sub>3</sub><sup>+</sup> counterions (their PZC is 7.2). The ionic strength was ~ 2 10<sup>-2</sup> mol/L. The  $\zeta$



1 potential of the nanoparticles, measured on a commercial setup (Delta Nano C, Beckman Coulter,  
2 France), was + 60mV.  
3

4  
5 These synthesis processes enabled us to get large amounts of the different suspensions, as we  
6 obtained several hundreds of ml of each batch with a  $\Phi_{\text{mag}}$  higher than 0.02.  
7  
8

#### 9 10 - *Transfer in DMAc solvent by dialysis*

11  
12 The magnetic nanoparticles were then transferred by dialysis in the dimethylacetamide (DMAc), a  
13 polar solvent ( $\epsilon_r = 37.8$ ) which is also a good solvent for the polystyrene (PS), the polymer used as a  
14 matrix for the nanocomposite. The initial aqueous suspension of  $\gamma\text{-Fe}_2\text{O}_3$  nanoparticles was placed in a  
15 dialysis bag made of regenerated cellulose with a MCWO Cut-off of 12000-14000 Da (Roth-Sochiel,  
16 France). The bag was then placed in a reservoir of DMAc (purity >99.9% %, Sigma Aldrich, France).  
17  
18 The dialysis enables to exchange progressively the molecules of the solvent, respectively water and  
19 DMAc, while keeping the colloidal stability. The DMAc bath was changed several times to exchange  
20 almost all molecules of water. We stopped the procedure of changing bath when such traces of water  
21 were low enough in the reservoir to allow the solubilization of chains of highly hydrophobic PS within  
22 the solvent.  
23  
24  
25  
26  
27  
28  
29  
30  
31  
32  
33  
34

35  
36 The  $\zeta$  potential of the nanoparticles after the transfer was still positive with a value of + 11mV.  
37

#### 38 39 - *Sample Preparation*

40  
41 The sample preparation process have been developed by Jouault et al. [Jouault 2009] for silica  
42 nanoparticles and adapted here to maghemite particles. We use polystyrene (PS, Aldrich, Mw 280000  
43 g/mol,  $I_p = 2$ , used as-received) as a matrix. The glass transition  $T_g$  of pure PS is around 100 °C. A  
44 concentrated solution of PS in DMAc (10% v/v) is mixed with a solution of maghemite nanoparticles  
45 previously transferred in DMAc, ranging from 0 to 5% v/v. The mixtures are stirred (using a magnetic  
46 rod) for 2 h. They are then poured into an aluminium cup and let cast in an oven at constant temperature  
47  
48  
49  
50  
51  
52  
53  
54  
55  
56  
57  
58  
59  
60  
 $T_{\text{cast}} = 130$  °C during 8 days. At the final stage, the residual solvent content inside the film is below 1%

1 w/w. This yields spherical dry films of 5 cm of radius and 0.1 cm of thickness (i.e., a volume of 1.9  
2 cm<sup>3</sup>).

3  
4  
5 - SAXS and SANS scattering

6  
7 The SAXS experiments on the nanocomposites and solutions were carried out at the SWING beamline  
8 at Soleil, using a sample changer enabling to load 10 samples simultaneously. SAXS measurements  
9 were recorded with the 2D AVIEX CCD camera, placed in the vacuum detection tunnel. 2 setups were  
10 used in order to obtain a large q-range. The sample to detector distance was fixed at 6.5m and 1.8m and  
11 a beamstop of 3 mm (vertical size) with a photodiode inserted in its center enabled us to measure the  
12 transmitted intensity. The experiments at 6.5m were repeated using a specially designed beamstop of 1  
13 mm in order to access very small q values:  $q_{\min} = 4.4 \cdot 10^{-4} \text{ \AA}^{-1}$ . The beamline energy was set to 7 keV for  
14 all experiments which enabled to obtain a large q range going from  $1.8 \cdot 10^{-3}$  to  $0.15 \text{ \AA}^{-1}$ , where  
15  $q = 2\pi \sin\theta / \lambda$ . The parasitic scattering from the air and mica windows was subtracted from the total  
16 scattering intensity. The resulting curves were normalized to take into account the effects related to the  
17 detector non-linearities and sample transmission. The 2D SAXS images obtained were radially averaged  
18 and corrected for the transmitted intensity using Foxtrot, the data reduction and analysis program  
19 developed at Soleil. In order to subtract the contribution of the PS chains in the nanocomposite samples,  
20 we have measured a pure PS matrix sample without magnetic nanoparticles  $I_{\text{pure\_PS}}$  and subtracted  $(1 -$   
21  $\Phi_{\text{mag}} * I_{\text{pure\_PS}})$  from all the nanocomposite samples. Concerning the liquid samples, both the scattering of  
22 the solvent  $I_{\text{solvent}}$  and the capillary  $I_{\text{capillary}}$  were removed by the subtraction of  $(1 - \Phi * I_{\text{solvent}} - I_{\text{capillary}})$  from  
23 all the solutions.  
24  
25

26  
27  
28  
29  
30  
31  
32  
33  
34  
35  
36  
37  
38  
39  
40  
41  
42  
43  
44  
45  
46  
47 SANS measurements were done on PACE spectrometer at LLB (LLB, Saclay, France). One  
48 configuration was used (Sample-Detector = 4.7m;  $\lambda = 6 \text{ \AA}$ ), covering a q-range from  $7 \cdot 10^{-3}$  to  $7 \cdot 10^{-2} \text{ \AA}^{-1}$ .  
49  
50 All measurements were done under atmospheric pressure and at room temperature. Standard corrections  
51 for sample volume, neutron beam transmission, empty cell signal subtraction, detector efficiency,  
52 subtraction of incoherent scattering and solvent buffer were applied to get the scattered intensities in  
53 absolute scale [25].  
54  
55  
56  
57  
58  
59  
60

### *- Transmission Electronic Microscopy*

In order to complete on a larger scale the SAS analysis of the nanocomposite structure, conventional TEM observations were also performed on the composite materials. The samples were cut at room temperature by ultramicrotomy using a Leica Ultracup UCT microtome with a diamond knife. The cutting speed was set to  $0.2 \text{ mm s}^{-1}$ . The thin sections of about 40 nm thickness were floated on deionized water and collected on a 400 mesh copper grid. Transmission electron microscopy was performed on a Tecnai F20 ST microscope (field-emission gun operated at 3.8 kV extraction voltage) operating at 200 kV. Precise observations of various regions of the sample were systematically done, starting at a small magnification which was then gradually increased. The sections observed were stable under the electron beam. The sample aspect remained similar on the whole area and for all pieces. Except for a few cutting scratches, moderate buckling, very rare bubbles, and impurities, the pictures presented below are completely representative of the single aspect of the sample, which thus appears homogeneous.

## **III Obtaining stable binary mixtures of magnetic nanoparticles and PS polymeric chains**

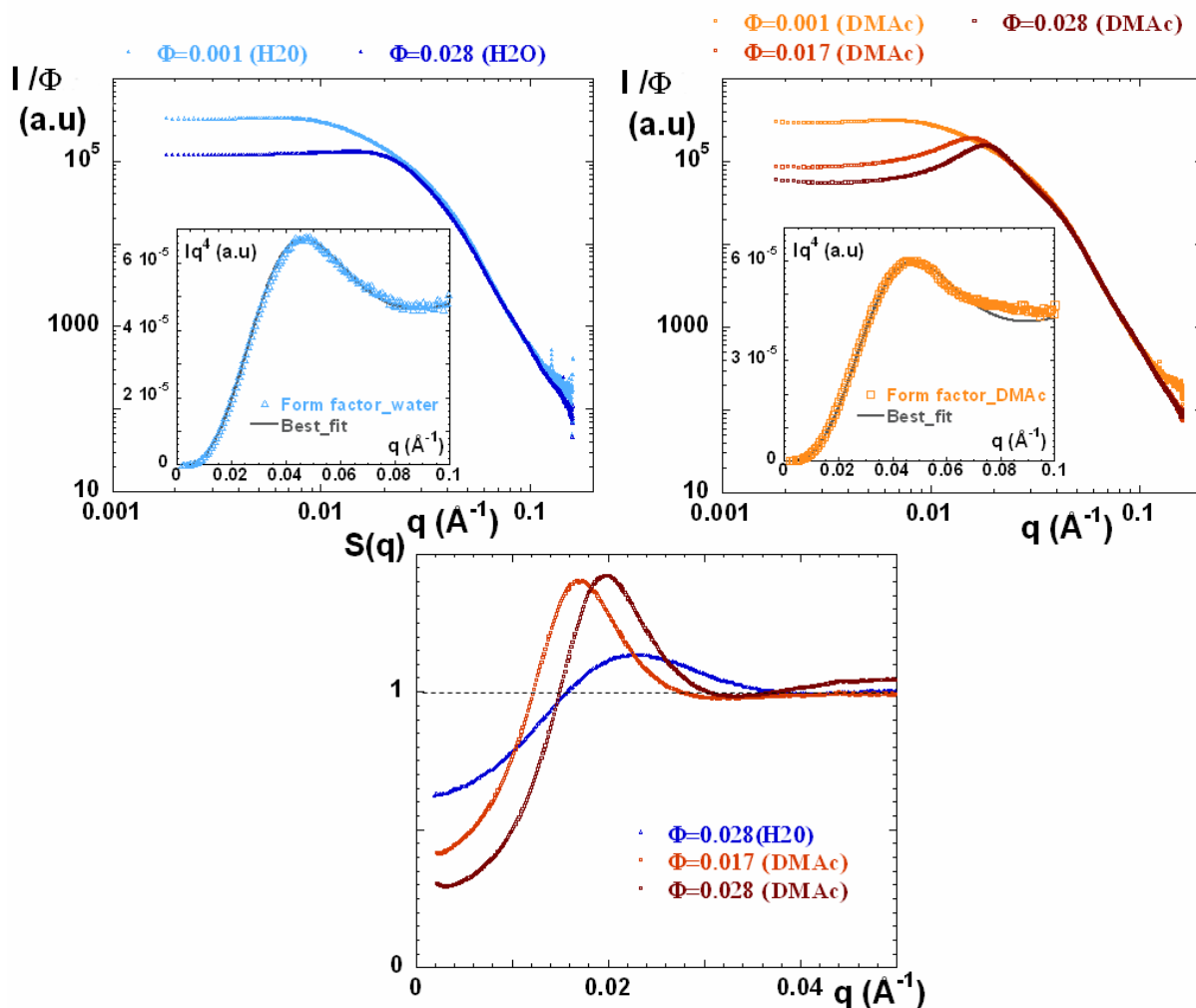
### ***1 Transfer and stability of $\gamma\text{-Fe}_2\text{O}_3$ magnetic nanoparticles in DMAc***

It has been demonstrated that DMAc enables a good control of the aggregation of the silica nanoparticles in the PS matrix [5]. Thus the film processing needs a first step of transfer of naked  $\gamma\text{-Fe}_2\text{O}_3$  nanoparticles, initially in water, to the organic medium. However, the transfer of such  $\gamma\text{-Fe}_2\text{O}_3$  nanoparticles in DMAc has never been reported. We present in this section how we achieved it and checked the stability of the nanoparticles by SAXS.

#### ***1.1 Structure of acidic aqueous suspensions of $\gamma\text{-Fe}_2\text{O}_3$ magnetic nanoparticles***

1 Prior to the transfer in DMAc, we have first checked by SAXS the stability of the aqueous suspensions  
 2 and determined the nanoparticles size for the four batches of particles. These four batches will be  
 3 denoted hereafter A, B, C and D.  
 4  
 5  
 6

7 The suspensions were measured at 2 different volume fractions of maghemite nanoparticles  $\Phi_{\text{mag}}$ :  
 8 immediately after the size-sorting process at  $\Phi_{\text{mag}} = 0.028$  and a dilute one at  $\Phi_{\text{mag}} = 0.001$ . The initial  
 9 suspensions were diluted in distilled water. We show the results in Figure 1.a for nanoparticles C. The  
 10 results for the other batches are very similar and are presented in the Supporting Information (Figures  
 11  
 12  
 13  
 14  
 15  
 16  
 17  
 18  
 19  
 20  
 21  
 22  
 23  
 24  
 25  
 26  
 27  
 28  
 29  
 30  
 31  
 32  
 33  
 34  
 35  
 36  
 37  
 38  
 39  
 40  
 41  
 42  
 43  
 44  
 45  
 46  
 47  
 48  
 49  
 50  
 51  
 52  
 53  
 54



55 Figure 1: (a) SAXS scattering curves for the suspensions of nanoparticles C in water. Inset:  $q^4 I(q)$   
 56 versus  $q$  for  $\Phi_{\text{mag}} = 0.001$  in water. The full line corresponds to the best fit of the form factor. (b) SAXS  
 57  
 58  
 59  
 60

scattering curves for the suspensions of nanoparticles C in DMAc. Inset:  $q^4 I(q)$  versus  $q$  for  $\Phi_{\text{mag}} = 0.001$  in DMAc. The full line corresponds to the best fit of the form factor. (c) Comparison of the structure factors of the concentrated suspensions of nanoparticles C in water and in DMAc.

Since the spherical nanoparticles are centrosymmetrical, their scattering is written as follow:

$$I(q) = \Phi_{\text{mag}} (\rho_{\text{mag}} - \rho_{\text{solv}})^2 V_{\text{NP}} P_{\text{NP}}(q) S(q) \quad (1)$$

where  $\rho_{\text{mag}}$  and  $\rho_{\text{solv}}$  are the respective scattering electronic density of maghemite and solvent (water or DMAc),  $V_{\text{NP}}$  is the volume of the nanoparticles,  $P_{\text{NP}}(q)$  their form factor and  $S(q)$  the structure factor.

For very dilute solutions, *i.e.* when  $\Phi_{\text{mag}} = 0.001$ , we assume that the interactions between the nanoparticles are negligible and thus  $S(q)$  is equal to 1 on all the probed  $q$ -range. This measurement allows us to determine  $P_{\text{NP}}(q)$  that gives the size and shape of the nanoparticles. The plateau obtained at low  $q$  in the Guinier range ( $q < 0.01 \text{ \AA}^{-1}$ ) confirms that the interactions between particles can be almost neglected. At large  $q$  ( $q > 0.06 \text{ \AA}^{-1}$ ) in the so-called Porod regime,  $I(q)$  roughly decreases like  $q^{-4}$ , which is characteristic of solid particles with a sharp interface. No oscillations are obtained in the form factor, indicating that the size distribution of the complexes is polydisperse.  $P_{\text{NP}}(q)$  is modelled by the form factor of a sphere with a lognormal distribution of median radius  $R_0$  and polydispersity  $\sigma$  :

$$V_{\text{NP}} P_{\text{NP}}(q) = \frac{\int_0^{\infty} \frac{4}{3} \pi R^3 \left( 3 \frac{\sin(qR) - qR \cos(qR)}{(qR)^3} \right)^2 R^3 P(R) dR}{\int_0^{\infty} R^3 P(R) dR} \quad \text{with } P(R) = \frac{1}{\sqrt{2\pi}\sigma R} \exp \left[ -\frac{1}{2\sigma^2} \left( \ln \frac{R}{R_0} \right)^2 \right] \quad (2)$$

The mean diameter of the nanoparticles  $R_{\text{NP\_mean}}$  is obtained from  $R_{\text{NP\_mean}}^3 = R_0^3 e^{\frac{9}{2}\sigma^2}$ . The best fit is presented in the inset of Figure 1, in a  $I(q)q^4 = f(q)$  representation. A maximum appears at a  $q$  position which is directly linked to the average radius of the spheres.  $R_0$  and  $\sigma$  can be unambiguously determined because  $R_0$  is linked to the peak  $q$ -position and  $\sigma$  to the adjustment of the shape of the peak. The results

for all sizes are presented in Table 1. They are compared with the ones obtained from magnetization measurements. The magnetization curves are presented in Figure SI.2 of the Supporting Information. Results from the two techniques are in excellent agreement. The four batches have close polydispersities and different  $R_{NP\_mean}$  ranging from 37 Å to 65 Å, proving that the size-sorting process has been successful.

	$R_0$ (Å) ; $\sigma$ (SAXS)	$R_0$ (Å) ; $\sigma$ (magnetization)	$R_{NP\_mean}$ (Å) (SAXS)
<b>A</b>	$32 \pm 1$ ; 0.32	$33 \pm 1$ ; 0.29	$37 \pm 2$
<b>B</b>	$38 \pm 1$ ; 0.32	$38 \pm 1$ ; 0.32	$45 \pm 2$
<b>C</b>	$44 \pm 1$ ; 0.32	$45 \pm 1$ ; 0.27	$51 \pm 2$
<b>D</b>	$54 \pm 1$ ; 0.32	$52 \pm 1$ ; 0.34	$65 \pm 2$

Table 1: Size characteristics of the different batches  $\gamma$ -Fe<sub>2</sub>O<sub>3</sub> nanoparticles obtained by SAXS and magnetization measurements.

The scattering curves of the suspensions for the dilute and concentrated volume fractions superimpose at large  $q$  in the Porod regime ( $I(q)/\Phi\Delta\rho = f(q)$ ) to the one at  $\Phi_{mag} = 0.001$ . This is due to the fact that only the form factor is probed in the Porod regime. However, for  $\Phi_{mag} = 0.028$ , the scattering curve has a different behavior at low  $q$ . It presents a soft maximum around  $0.02 \text{ \AA}^{-1}$ . This comes from the interparticle interactions which are no longer negligible and the structure factor  $S(q)$  in equation (1) is no more equal to 1. This structure factor is presented in Figure 1.c. It is calculated by dividing the total scattering by the form factor of the nanoparticles. It is equal to 1 at large  $q$ , it shows a correlation peak at intermediate  $q$  and it tends to a value inferior to 1 when  $q \rightarrow 0$ . In the thermodynamic limit (for  $q \rightarrow 0$ ), it tends to the isothermal osmotic compressibility of the system. Its decay to a value inferior to 1 when going towards very low  $q$  means that the interparticle interactions are repulsive on average. The

nanoparticles must thus be homogeneously dispersed in the suspension and the correlation peak of the structure factor at  $q^* \sim 0.022 \text{ \AA}^{-1}$  should correspond in real space to the mean interparticle distance between the nanoparticles  $d_{\text{mean}}$ . In this case,  $2\pi/q^*$  must be equal to  $d_{\text{mean}} = (2R_{\text{NP\_mean}})^3 \sqrt{\frac{\pi}{6\Phi_{\text{mag}}}}$  as  $\Phi_{\text{mag}} = V_{\text{NP\_mean}}^3/d_{\text{mean}}^3$ . For  $\Phi_{\text{mag}} = 0.028$ , one gets  $d_{\text{mean}} = 285 \text{ \AA}$  from the measurement ( $q_{\text{max}} \sim 0.022 \text{ \AA}^{-1}$ ) and  $272 \text{ \AA}$  from the calculation. The excellent agreement between those two estimations confirms the perfect dispersion of the nanoparticles.

These results are in agreement with the values of the 2<sup>nd</sup> Virial coefficients of similar suspensions obtained by osmotic measurements [26]. In such suspensions of naked ( $\gamma\text{-Fe}_2\text{O}_3$ ) nanoparticles in aqueous acidic medium, there are three main interactions that contribute to the interparticular potential [26, 27]: (i) short-range Van der Waals attractions, (ii) magnetic dipolar interactions, which are found to be globally attractive if the anisotropic interparticle potential is integrated over all directions. They vary from  $-1/r^6$  to  $-1/r^3$  depending on the strength of the magnetic coupling  $\gamma = (\mu_0/kT)(\mu_1\mu_2/r^3)$  between two nanoparticles of respective momentum  $\mu_1$  and  $\mu_2$ . Finally there are (iii) the coulombian electrostatic repulsions at longer range described by a Yukawa potential according to the DLVO theory [28] :

$$\frac{V_{el}(r)}{kT} = \frac{Z_{\text{NP}}^2 e^2}{4\pi\epsilon_r\epsilon_0 k_B T} \frac{e^{-\kappa r}}{r} \text{ where } \kappa = \sqrt{\frac{2e^2 I}{\epsilon_r\epsilon_0 k_B T}} \quad (3)$$

where  $Z_{\text{NP}}$  is the number of charges carried by the nanoparticles,  $e$  the elementary charge of an electron,  $\epsilon_0$  the permittivity of the vacuum,  $\epsilon_r$  the relative permittivity of the medium (78.5 in water),  $k_B$  the Boltzmann constant,  $T$  the temperature,  $\kappa$  the inverse of the Debye length and  $I$  the ionic strength defined by  $I = \frac{1}{2} \sum_i c_i z_i^2$  ( $c_i$  is the concentration of the ionic specie  $i$  and  $Z_i$  its valency).

In our experimental conditions at pH 2, the surface of the nanoparticles is strongly positively charged as its  $\zeta$  potential equals + 60 mV. As a result the coulombic repulsions are sufficiently important to overcome the attractive interactions at moderate ionic strength. As shown in Figure S.I 1 in Supporting Information, the sum of the interactions in all the aqueous suspensions from the different batches is

1 always repulsive, even for the largest nanoparticles D, although the attractive interactions strongly  
2 increase with size.  
3  
4  
5  
6

### 7 *1.2 Structure of the suspensions of $\gamma$ -Fe<sub>2</sub>O<sub>3</sub> magnetic nanoparticles in DMAc*

8  
9

10 After the solvent transfer of the naked ( $\gamma$ -Fe<sub>2</sub>O<sub>3</sub>) nanoparticles, the interparticular potential is much  
11 more repulsive in DMAc than in water because the soft maximum associated to the correlation peak of  
12 the structure factor is much marked, as shown by the SAXS scattering curves of Figure 1.b. This is  
13 highlighted in Figure 1.c which compares the structure factor at  $\Phi_{\text{mag}} = 0.028$  in DMAc to the one at  
14  $\Phi_{\text{mag}} = 0.028$  in water. The correlation peak at  $q^*$  is much more pronounced as it reaches a value of 1.4  
15 in DMAc while it was around 1.15 in water. Accordingly, the isothermal osmotic compressibility has  
16 been strongly reduced because  $S(q)_{q \rightarrow 0}$  tends to a much lower value.  
17  
18  
19  
20  
21  
22  
23  
24  
25  
26

27 We have also checked that a dilution in pure DMAc of the suspension after dialysis does not affect its  
28 stability by comparing in figure 1.c the structure factor of a suspension at  $\Phi_{\text{mag}} = 0.017$  with the one at  
29  $\Phi_{\text{mag}} = 0.028$ . Both structure factors look very similar. As  $d_{\text{mean}}$  increases with dilution, the correlation  
30 peak is shifted towards low  $q$ . The height of the correlation peak is slightly lower for  $\Phi_{\text{mag}} = 0.017$ .  
31  $S(q)_{q \rightarrow 0}$  has a higher value for  $\Phi_{\text{mag}} = 0.017$ , in accordance with the fact that the isothermal osmotic  
32 compressibility decreases when increasing  $\Phi_{\text{mag}}$ , in a case of repulsive interparticle interactions on  
33 average. At very low  $\Phi_{\text{mag}}$ , please note that the form factor of the nanoparticle is the same after the  
34 transfer in the organic solvent.  
35  
36  
37  
38  
39  
40  
41  
42  
43  
44  
45

46 In DMAc, the attractive interactions in the system are close to the ones in water. The magnetic dipolar  
47 interactions, that depend only on  $R_{\text{NP\_mean}}$ , are exactly similar while the Van der Waals attractions are of  
48 the same order (the Hamaker constant is slightly changed because the relative permittivity of DMAc is  
49 around twice lower than the one of water). The strong changes in the interparticular potential are thus  
50 related to an important increase of the electrostatic repulsions. The nanoparticles indeed still bear a  
51 positive charge because the  $\zeta$  potential was still measurable at + 11 mV. The high dielectric constant of  
52  
53  
54  
55  
56  
57  
58  
59  
60



1  
2  
3  
4  
5  
6  
7  
8  
9  
10  
11  
12  
13  
14  
15  
16  
17  
18  
19  
20  
21  
22  
23  
24  
25  
26  
27  
28  
29  
30  
31  
32  
33  
34  
35  
36  
37  
38  
39  
40  
41  
42  
43  
44  
45  
46  
47  
48  
49  
50  
51  
52  
53  
54  
55  
56  
57  
58  
59  
60

DMAc enables the dissociation of the Fe-OH groups at the nanoparticles surface. The surface charge of the nanoparticles has nevertheless been strongly reduced compared to the acidic aqueous suspension as  $\zeta$  was reduced from + 60 mV down to +11 mV. However the dialysis procedure with several baths in pure DMAc had progressively washed away all ions and the ionic strength  $I$  at the end of the transfer is close to 0 (only the nanoparticles counterions ensure the electroneutrality of the suspension). Thus, during the transfer process, the strong reduction of  $I$  combined with the decrease of  $\epsilon_r$  overcompensate the decrease of  $Z_{NP}$ , which globally increase the electrostatic repulsions. Please note that the elimination of the ionic strength by the use of dialysis to transfer the solvent is crucial. We tried to exchange the solvents by evaporating the water on mixtures of acidic aqueous suspensions and DMAc by simple boiling. It always leads to flocculation during the process because the salt was not removed but progressively concentrated.

As for the aqueous suspensions, we checked that the sum of the interactions of the suspensions with the four different sizes of nanoparticles in DMAc was repulsive (see Figure S.I 1 in Supporting Information).

## ***2 Effect of the addition of PS chains on the suspensions of $\gamma$ -Fe<sub>2</sub>O<sub>3</sub> magnetic nanoparticles in DMAc***

Prior to the processing of the films, we have studied the influence of the addition of a large amount of PS chains on the colloidal stability of  $\gamma$ -Fe<sub>2</sub>O<sub>3</sub> nanoparticles suspensions in DMAc. We have measured by SANS the scattering of a suspension of nanoparticles C at  $\Phi_{mag} = 0.015$  in which we added a quantity of PS chains (10% v/v). The scattering signal of the PS chains was matched to get only the scattering of the maghemite nanoparticles. The measurements were performed in a mixture of 15% of deuterated DMAc (Euristop France) and 85 % of hydrogenated DMAc which has a neutron scattering length density  $\rho_{mixture}$  of  $1.43 \cdot 10^{-10} \text{ cm}^{-2}$  that exactly matches the one of hydrogenated PS. The nuclear scattering length density of maghemite  $\rho_{\gamma\text{-Fe}_2\text{O}_3}$  has a very different value ( $6.96 \cdot 10^{-10} \text{ cm}^{-2}$ ), which enabled a measurement of the scattering of the nanoparticles alone with a good statistics.

The scattering intensity of the maghemite nanoparticles in the DMAc suspension with contrast-matched PS chains is presented in the inset of Figure 2. It can be described as presented in Equation 1, by a product of a form factor and a structure factor. The structure factor is displayed in figure 2 where it is compared to the one of a suspension with a close  $\Phi_{\text{mag}}$  (0.017) in pure DMAc solution presented in previous section.

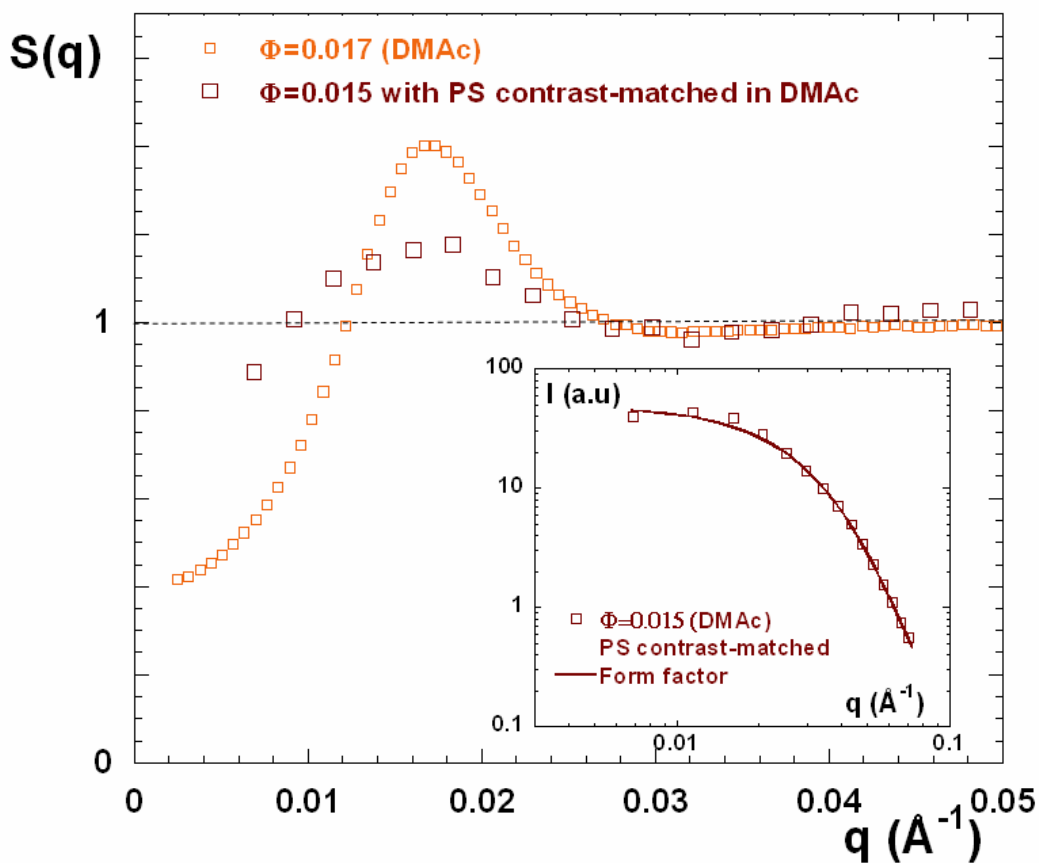


Figure 2: Comparison of the structure factors of the suspensions of nanoparticles C with close  $\Phi_{\text{mag}}$  either in pure DMAc solution or with 10% v/v of contrast-matched PS chains. Inset: SANS scattering of suspensions of nanoparticles C with  $\Phi_{\text{mag}} = 0.015$  in DMAc with 10% v/v of contrast-matched PS chains. The full line corresponds to the form factor.

It clearly appears that the introduction of the PS chains has changed the interparticle potential between the nanoparticles in the system. The two structure factors have the characteristic features of

1 repulsive systems ( $S(q)_{q \rightarrow 0} < 1$  and a correlation peak at intermediate  $q$ ) with rather similar  
2 concentrations. For the suspension with contrast-matched PS chains,  $q^*$  is slightly shifted towards the  
3 low  $q$  compared to the suspension in pure DMAc because  $\Phi_{\text{mag}}$  is slightly lower (0.015 versus 0.017).  
4  
5  
6  
7 However, the repulsions are much less marked when PS chains are introduced in solution. The height of  
8 the correlation peak at  $q^*$ , directly linked to the intensity of the repulsions, decreases from a value of  $\sim$   
9 1.4 in pure DMAc to a value of  $\sim 1.15$  with 10%v/v of PS chains. Accordingly, the isothermal osmotic  
10 compressibility is higher as  $S(q)_{q \rightarrow 0}$  increases from a  $\sim 0.4$  in pure DMAc up to  $\sim 0.8$  with the PS chains.  
11  
12  
13  
14  
15  
16

17 As the nanoparticles are still in repulsive regime when PS chains are introduced, there are thus no  
18 specific interactions between the naked maghemite nanoparticles and PS which would have led to  
19 aggregation via a bridging process. The change in the interparticular potential can result from the  
20 following changes in the effective interactions between nanoparticles. First, as the content of PS chains  
21 is very important, the effective dielectric constant of the binary mixture of DMAc and PS chains is  
22 reduced compared to the one of the pure DMAc because  $\epsilon_r \sim 3$  for PS. This can both increase the Van  
23 der Waals attractions and decrease the electrostatic repulsions by changing the dissociation of the  
24 charges at the surface of the naked nanoparticles. Second, the presence of the PS chains can induce some  
25 depletion attractive interactions. However these depletion attractions must have a very limited range. As  
26 the PS chains are in semi-dilute regime with a very high concentration, the typical size of the system is  
27 the mesh size of the blob  $\xi$  of the semi-dilute solution, around  $11 \text{ \AA}$  here [29]. The range of the depletion  
28 interactions is thus necessarily lower than such a value.  
29  
30  
31  
32  
33  
34  
35  
36  
37  
38  
39  
40  
41  
42  
43  
44

45 Despite the reduction of the effective repulsions between the nanoparticles in presence of PS chains,  
46 our experimental system proves to be a good candidate for forming a nanocomposite with controlled  
47 aggregation due to its weak repulsive structure prior to the drying.  
48  
49  
50  
51  
52  
53  
54

#### 55 **IV Structures of aggregates of magnetic nanoparticles in nanocomposites polymeric films**

56  
57  
58  
59  
60

1  
2  
3  
4  
5  
6  
7  
8  
9  
10  
11  
12  
13  
14  
15  
16  
17  
18  
19  
20  
21  
22  
23  
24  
25  
26  
27  
28  
29  
30  
31  
32  
33  
34  
35  
Several nanocomposite films were obtained for the four different types of nanoparticles and over a large range of  $\Phi_{\text{mag}}$  (calculated in this section after evaporation of the DMAc solvent) on almost four decades ranging from  $10^{-5}$  up to 0.05. The films had a surface of  $\sim 80 \text{ cm}^2$  and a typical thickness ranging from 0.5 to 1 mm. Their aspect was macroscopically homogeneous. As the maghemite optically absorbs in the red, the films diluted in  $\gamma\text{-Fe}_2\text{O}_3$  nanoparticles were red/orange while the most concentrated were black. As reported on the system close to this one, made of silica nanoparticles dispersed in PS matrix [5], there were microcracks at the surface of the films. We describe in this section how we obtained the main structure of the aggregates of  $\gamma\text{-Fe}_2\text{O}_3$  nanoparticles by SAXS and TEM microscopy first by focusing on a single nanoparticle size (sample C) and in a second step, how a change of the initial size of the nanoparticles tunes the aggregation. X-rays scattering is mainly dominated by the contrast between the inorganic particles and the polymer. It directly depends on the particles' concentration in the polymer matrix. Only the powerful high resolution available in the setup of a SAXS apparatus in the synchrotron source enables to determine the structure of filled nanocomposites at the very low nanoparticle content range probed here.

### 36 ***1 Typical features of the scattering of $\gamma\text{-Fe}_2\text{O}_3$ nanoparticles in the nanocomposites polymeric films***

37  
38  
39  
40  
41  
42  
43  
44  
45  
46  
47  
48  
49  
50  
51  
52  
53  
54  
55  
56  
57  
58  
59  
60  
We present in this section the main features of the scattering curves of the  $\gamma\text{-Fe}_2\text{O}_3$  nanoparticles within the polymeric matrix obtained by SAXS. They are shown in Figure 3 for the nanoparticles C for

$\Phi_{\text{mag}}$  ranging from  $10^{-5}$  to 0.05.

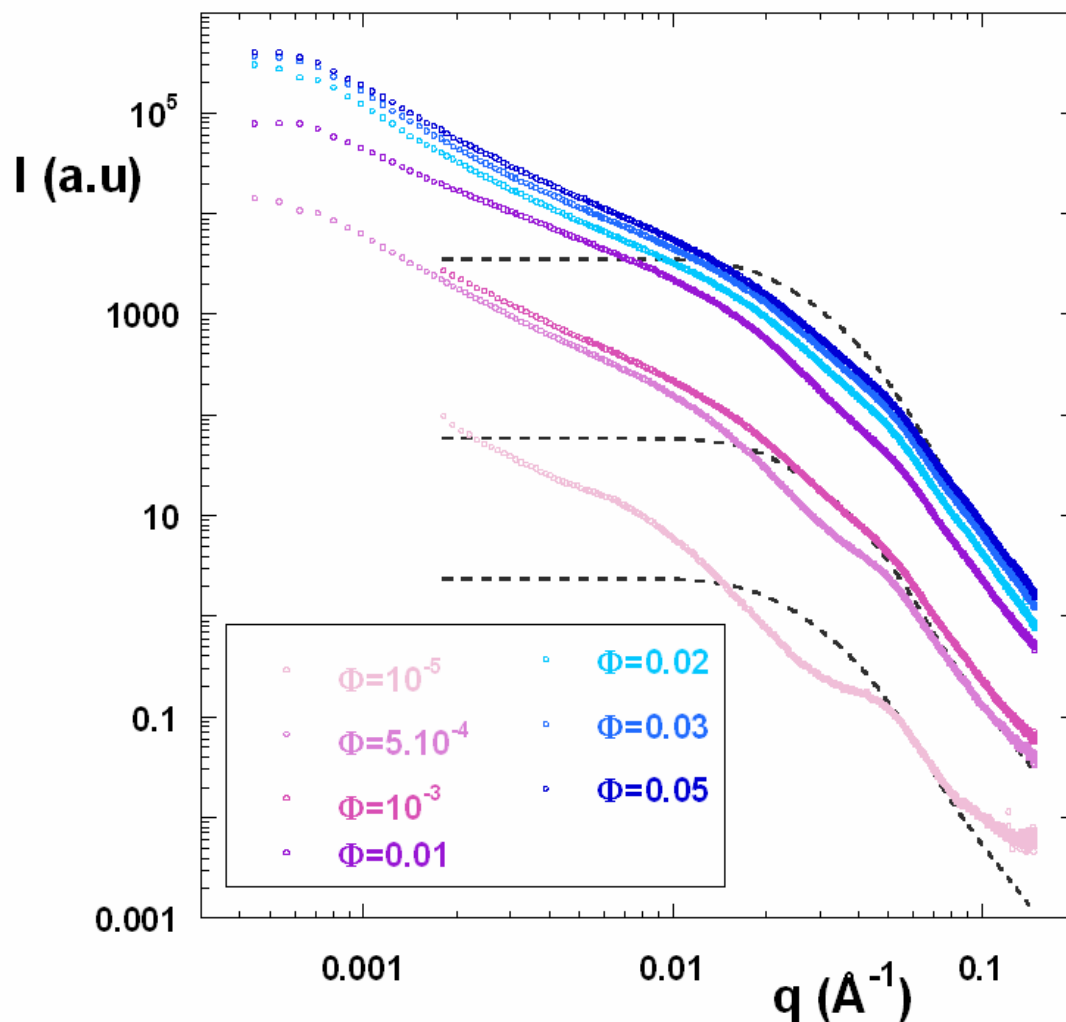


Figure 3: SAXS scattering curves of the  $\gamma\text{-Fe}_2\text{O}_3$  nanoparticles in the PS polymeric matrix obtained by SAXS for nanoparticles C. The dashed lines correspond to the form factor of the nanoparticles.

Irrespective of the nanoparticles size and  $\Phi_{\text{mag}}$ , all the scattering curves present a  $q^{-4}$  decay at large  $q$  ( $q > 0.1 \text{\AA}^{-1}$ ) corresponding to the surface scattering of the individual nanoparticles. All the scattering curves perfectly superimpose to the form factors of the nanoparticles measured in section III.1.

At lower  $q$ , two distinct behaviors appear depending on  $\Phi_{\text{mag}}$ :

1 - For  $\Phi_{\text{mag}} \leq 10^{-4}$ , there is a correlation peak in the range  $0.05 \text{ \AA}^{-1} - 0.08 \text{ \AA}^{-1}$ . Its q-position corresponds  
 2 exactly to  $2\pi/(2R_{\text{NP\_mean}})$ , *i.e.* to the contact between 2 nanoparticles in real space. At lower q, the  
 3 scattering presents a strong decay (between  $q^{-3}$  and  $q^{-4}$ ) and bends toward a Guinier regime around  $q \sim$   
 4  $0.008 \text{ \AA}^{-1}$ , indicating that the aggregates have a finite size. At lower q, depending on the samples, there  
 5 is eventually an upturn at very low q with a  $q^{-3}$  behavior.  
 6  
 7  
 8  
 9

10 - For  $\Phi_{\text{mag}} \geq 5 \cdot 10^{-4}$ , the scattering spectra look different. The correlation peak still exists in the  
 11 range  $5 \cdot 10^{-3} < \Phi_{\text{mag}} < 10^{-2}$  but less pronounced. For higher  $\Phi_{\text{mag}}$ , it is also present but looks more like a  
 12 break of slope. At intermediate q, the scattering increases rather strongly again and, around  $0.025 \text{ \AA}^{-1}$ ,  
 13 there is a net break of slope for all samples and all  $\Phi_{\text{mag}}$ . The scattering decays like  $q^{-1.7}$  (in the q- range  
 14  $0.0008 \text{ \AA}^{-1} - 0.008 \text{ \AA}^{-1}$ ). At very low q, ( $q < 0.0008 \text{ \AA}^{-1}$ ), the scattering tends towards a Guinier regime,  
 15 indicating that the aggregates have a finite size.  
 16  
 17  
 18  
 19  
 20  
 21  
 22  
 23  
 24  
 25  
 26

27 This first qualitative description indicates that the overall size of the aggregate is much larger in the  
 28 high  $\Phi_{\text{mag}}$  regime than in the low  $\Phi_{\text{mag}}$  one, because the Guinier regime is reached at much lower q. As  
 29 the correlation peak is present for all  $\Phi_{\text{mag}}$ , with a q-position corresponding to two nanoparticles in close  
 30 contact, it is likely that the aggregates present at low  $\Phi_{\text{mag}}$ , that will be named hereafter ‘primary  
 31 aggregates’, are in fact present for all  $\Phi_{\text{mag}}$ . They must then form aggregates of primary aggregates at  
 32 higher  $\Phi_{\text{mag}}$  that we will describe in the following by ‘supra-aggregates’. We present in the next sections  
 33 a quantitative analysis of the structure of the supra-aggregates realized in the framework of such a  
 34 hypothesis.  
 35  
 36  
 37  
 38  
 39  
 40  
 41  
 42  
 43  
 44  
 45  
 46  
 47  
 48

## 49 ***2 Structure of supra-aggregates from the combined analysis of SAXS scattering and TEM*** 50 ***experiments*** 51 52 53 54 55

### 56 ***2.1 Nanocomposites at $\Phi_{\text{mag}} \leq 10^{-4}$ : Scattering of primary aggregates*** 57 58 59 60

Concerning the primary aggregates, the intensity of the correlation peak at  $q_{\text{peak}} = 2\pi/(2R_{\text{NP\_mean}})$  indicates that the contact distance between two nanoparticles is strongly favored in the sample. The primary aggregate must thus be composed of dense clusters of several nanoparticles. This is confirmed in Figure 4.c that presents a TEM picture of such a primary aggregate obtained with nanoparticles C at  $\Phi_{\text{mag}} = 10^{-5}$ . This picture is representative of the aggregates that are observed on the whole TEM grid with a very low content. This explains why the scattering decay of the primary aggregate at intermediate  $q$  lies between  $q^{-3}$  and  $q^{-4}$ , as one probes the surface scattering of a dense object. The Guinier regime at low  $q$  and the decay at intermediate  $q$  can thus be described by the form factor of polydisperse spheres.

However this does not explain the  $q^{-3}$  upturn observed at very low  $q$ . It could arise from the presence of a limited number of larger aggregates but none are observed on the whole TEM grid (Figure 4.c). The  $q^{-3}$  upturn indeed comes from the scattering of microcracks present in the sample, which decay like  $q^{-3}$ , as it has been shown in [30]. Even after the subtraction of the pure PS matrix (see the Materials and Methods section), there remains some scattering signal of microcracks because their scattering behavior is modified by the presence of the nanoparticles. At low  $q$ , the whole scattering can thus be described by the linear combination of a form factor of polydisperse spheres and of a  $q^{-3}$  decay with a  $K$  prefactor:

$$I(q) = \Phi_{\text{mag}} (\rho_{\text{mag}} - \rho_{\text{PS}})^2 \frac{\int_0^{\infty} \frac{4}{3} \pi R^3 \left( 3 \frac{\sin(qR) - qR \cos(qR)}{(qR)^3} \right)^2 R^3 P(R) dR}{\int_0^{\infty} R^3 P(R) dR} + Kq^{-3} \quad (4) \quad \text{where}$$

$P(R)$  accounts for the same lognormal law as in equation (2). However, the median radius is here the one of the primary aggregate  $R_{\text{PA}_0}$ . Accordingly, we deduce the mean radius of the primary aggregates

$$R_{\text{PA\_mean}} \text{ from } R_{\text{PA\_mean}}^3 = R_{\text{PA}_0}^3 e^{\frac{9}{2}\sigma^2}.$$

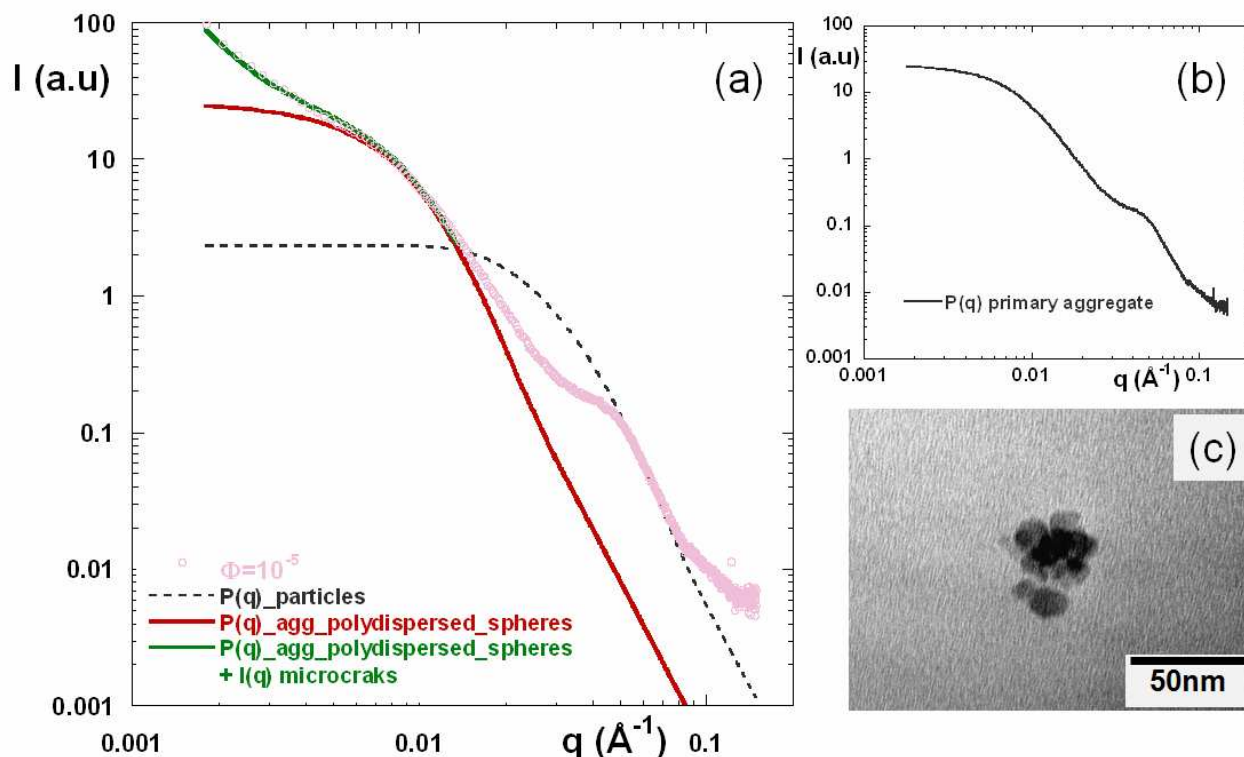


Figure 4: (a) Scattering of primary aggregates of nanoparticles C at  $\Phi_{\text{mag}} = 10^{-5}$ , decomposed at low  $q$  in a linear combination of the form factor of polydisperse spheres and scattering of microcracks, compared with the form factor of the nanoparticles C at the same  $\Phi_{\text{mag}}$ . (b) Scattering of the form factor of primary aggregates of nanoparticles C. (c) TEM picture of a nanocomposite made of nanoparticles C at  $\Phi_{\text{mag}} = 10^{-5}$ .

It is shown in Figure 4.a how such a linear combination enables to perfectly modeled the low  $q$  scattering of the primary aggregate of nanoparticles C measured at  $\Phi_{\text{mag}} = 10^{-5}$  (for  $q < 0.02 \text{ \AA}^{-1}$ ). In the next sections, the form factor of the primary aggregate of nanoparticles C will be described by such a scattering curve after the subtraction of the microcracks scattering. It is shown in Figure 4.b.

The mean radius of the primary aggregate  $R_{\text{PA\_mean}}$  is  $168 \text{ \AA}$  ( $R_{\text{PA}_0} = 140 \text{ \AA}$ ;  $\sigma = 0.35$ ), about three times the mean diameter of the nanoparticles, in accordance with Figure 4.c.



As the scattering of an assembly of non-interacting centro-symmetrical objects can be described by equation 1, with  $S(q) = 1$  for all  $q$ , the value of  $I_{\text{objects}}(q=0)/\Phi\Delta\rho^2$  is a direct measurement of the volume of the object. This is true both for primary aggregates and for isolated nanoparticles. The direct comparison of the scattered intensity of primary aggregates  $I_{\text{PA}}(0)$  and of the scattered intensity of nanoparticles  $I_{\text{NP}}(0)$ , for same  $\Phi$  and  $\Delta\rho^2$  as shown in Figure 4.a, enables the measurement of the mean number of aggregation in the primary aggregates  $N_{\text{PA\_agg}}$  because  $I_{\text{PA}}(0) = N_{\text{PA\_agg}} I_{\text{NP}}(0)$ . We obtain  $N_{\text{PA\_agg}} \sim 10$  for the primary aggregate of nanoparticles C measured at  $\Phi_{\text{mag}} = 10^{-5}$ , here again in accordance with picture of Figure 4.c.

Finally, we can measure the compactness of the primary aggregates because the inner volume fraction of nanoparticles within the primary complexes  $\Phi_{\text{PA\_inner}}$  is obtained from:

$$\Phi_{\text{PA\_inner}} = N_{\text{PA\_agg}} \left( \frac{R_{\text{NP\_mean}}}{R_{\text{PA\_mean}}} \right)^3 \quad (5)$$

We get  $\Phi_{\text{PA\_inner}} = 0.3$ . This high value confirms that the primary aggregates are dense clusters and explains why they scatter at low  $q$  like dense polydisperse spheres.

It is worth noting that a similar scattering behavior of dense clusters of few nanoparticles has also been reported by Fresnais et al [31] on different systems of polymer/inorganic nanoparticles co-assemblies. Although there is no analytic form for the scattering signal of such dense small clusters made of polydisperse spheres, the authors have shown that the scattering features of such clusters can be perfectly recovered by reverse Monte-Carlo simulations.

## 2.2 Nanocomposites at $\Phi_{\text{mag}} \geq 5 \cdot 10^{-4}$ : Scattering of supra-aggregates

We detail here the scattering of the supra-aggregates made of primary aggregates. First of all, let us note that the scattering of the microcracks is here negligible compared to the one of the supra-aggregates because  $\Phi_{\text{mag}}$  is rather high. As the primary aggregates are dense 3-D objects, they are centro-symmetrical. The scattering of the supra-aggregates can thus be described like in equation 1 by the

product of the form factor of the primary aggregates and an effective structure factor between primary aggregates  $S_{\text{eff}}(q)$ . The  $S_{\text{eff}}(q)$  are plotted in Figure 5.a for nanoparticles C at various  $\Phi_{\text{mag}}$  ranging from  $5 \cdot 10^{-4}$  to  $5 \cdot 10^{-2}$ . They are calculated by dividing the scattered intensity by  $P(q)_{\text{prim\_agg}} \Phi_{\text{prim\_agg}} / \Phi_{\text{mag}}$ , where  $P(q)_{\text{prim\_agg}}$  is the form factor of the primary aggregate presented in Figure 4.b and  $\Phi_{\text{prim\_agg}}$  its volume fraction.

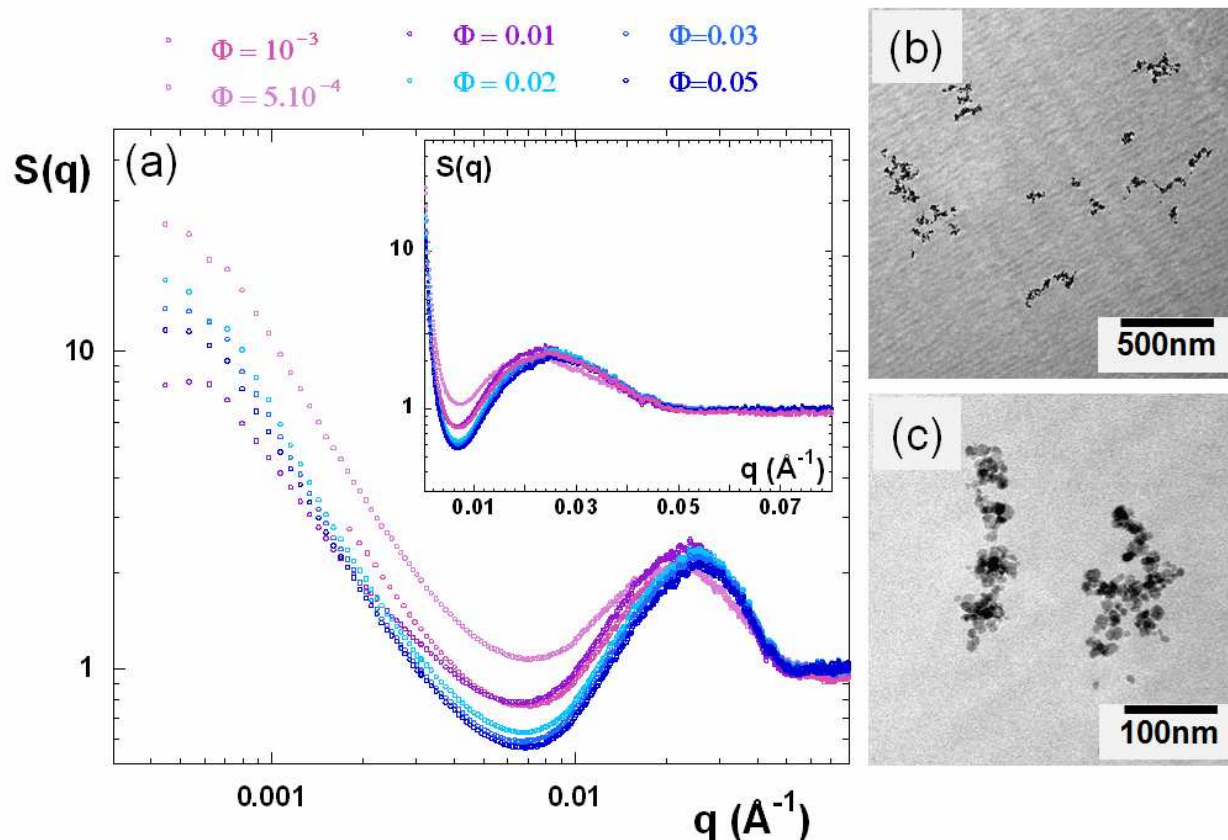


Figure 5: (a) Effective structure factor between the primary aggregates  $S_{\text{eff}}(q)$  for nanoparticles C. Inset: same  $S_{\text{eff}}(q)$  in log-linear scale. (b) TEM picture of a nanocomposite made of nanoparticles C at  $\Phi_{\text{mag}} = 5 \cdot 10^{-4}$ . (c) TEM picture of a nanocomposite made of nanoparticles C at  $\Phi_{\text{mag}} = 5 \cdot 10^{-4}$  with a higher magnification.

Very nicely,  $S_{\text{eff}}(q)$  is perfectly equal to 1 between  $0.05 \text{ \AA}^{-1}$  and  $0.08 \text{ \AA}^{-1}$  (see inset of Figure 5.a), in the  $q$ -region where the correlation peaks were observed (its  $q$ -value was  $0.06 \text{ \AA}^{-1}$ ). It proves that the mean number of aggregation of primary aggregates  $N_{\text{PA\_agg}}$  is exactly the same at every  $\Phi_{\text{mag}}$  from  $10^{-5}$

up to  $5 \cdot 10^{-2}$ . It validates the hypothesis of supra-aggregates formed by a hierarchical structure made of dense primary aggregates and organized at a higher scale in a more open way.

At lower  $q$ ,  $S_{\text{eff}}(q)$  shows a strong correlation peak at  $0.025 \text{ \AA}^{-1}$ . It roughly corresponds, in real space, to twice the mean radius of primary aggregates. This confirms again the hierarchical structure of the supra-aggregates with primary aggregates in close contact. In figure 3, the slope break observed in this  $q$ -range comes from the convolution of such correlation peak in  $S_{\text{eff}}(q)$  with the form factor of the primary aggregates that is still increasing when going towards low  $q$ .

In the  $q$ -region ranging from  $0.0008 \text{ \AA}^{-1}$  to  $0.008 \text{ \AA}^{-1}$ ,  $S_{\text{eff}}(q)$  decays like  $q^{-1.7}$ . The primary aggregates are organized within the supra-aggregates in a fractal way with a fractal dimension  $D^f$  of 1.7. Finally, at very low  $q$ , the scattering curves reach a Guinier regime. The supra-aggregates have a finite size. All of these features are observed in Figure 5.b and Figure 5.c showing TEM pictures of isolated supra-aggregates measured for nanoparticles C at  $\Phi_{\text{mag}} = 5 \cdot 10^{-4}$  with different magnifications.

The SAXS scattering enables to extract quantitative information on the supra-aggregates. In a similar way as we obtained the mean number of aggregated nanoparticles within the primary aggregates  $N_{\text{PA}_{\text{agg}}}$  in previous section, it is possible to obtain the mean number of aggregated primary aggregates within the supra-aggregates  $N_{\text{SA}_{\text{PA}_{\text{agg}}}}$ . The scattered intensity of supra-aggregates  $I_{\text{SA}}(0)$  is compared to the one of the primary aggregates  $I_{\text{PA}}(0)$ .  $N_{\text{SA}_{\text{PA}_{\text{agg}}}}$  can be directly obtained from Figure 5.a because it corresponds to  $S_{\text{eff}}(q)$  when  $q \rightarrow 0$ . We get here  $N_{\text{SA}_{\text{PA}_{\text{agg}}}} \sim 12 - 16$  for  $\Phi_{\text{mag}}$  higher than  $10^{-2}$  and a slightly larger value for  $\Phi_{\text{mag}} = 5 \cdot 10^{-4}$ . The mean number of total aggregation of nanoparticles within the supra-aggregates  $N_{\text{SA}_{\text{agg}}}$  is the product of  $N_{\text{PA}_{\text{agg}}}$  and  $N_{\text{SA}_{\text{PA}_{\text{agg}}}}$ . It is  $\sim 100$  for nanoparticles C. In the TEM pictures of Figure 5.b and 5.c, the supra-aggregates seem to contain less nanoparticles than we obtained from SAXS analysis. It is a misleading effect from TEM microscopy because the overall size of the supra-aggregates is larger than the thickness of the cut of the samples used (40 nm, see Materials and Methods section).

The values of  $D^f$ ,  $N_{\text{SA}_{\text{PA}_{\text{agg}}}}$  and  $R_{\text{PA}_{\text{mean}}}$  enable to get the mean radius  $R_{\text{SA}_{\text{mean}}}$  of supra-aggregates:

$$R_{SA\_mean} = N_{SA\_PA\_agg}^{1/D^f} R_{PA\_mean} \quad (6)$$

We obtain  $R_{SA\_mean} \sim 800 \text{ \AA}$ , similarly as observed in Figure 5.c.

As recalled in the Introduction section, one of the main dominant effects in the reinforcement mechanisms of nanocomposites is the network effect. It is thus important to be able to determine precisely the percolation threshold volume fraction in our nanocomposites. This can be done because all the structural dimensions of the system are quantitatively characterized. Let us determine the effective volume fraction occupied by spheres  $\Phi_{SA}$  with the radius of supra-aggregates  $R_{SA\_mean}$  as a function of  $\Phi_{mag}$  :

$$\Phi_{SA} = \frac{\Phi_{mag}}{N_{SA\_agg}} \left( \frac{R_{SA\_mean}}{R_{NP\_mean}} \right)^3 \quad \text{or} \quad \Phi_{SA} = \frac{\Phi_{mag}}{\Phi_{PA\_inner}} N_{SA\_PA\_agg}^{(3/D^f - 1)} \quad (7)$$

For the suspensions of nanoparticles C at  $\Phi_{mag} = 0.02$ ,  $\Phi_{mag} = 0.03$  and  $\Phi_{mag} = 0.05$ , one obtains respectively  $\Phi_{SA} = 0.60$ ,  $\Phi_{SA} = 0.79$  and  $\Phi_{SA} = 1.2$ .

If the supra-aggregates are homogeneously dispersed at large scale, the percolation threshold volume fraction is located at  $\Phi_{SA} \sim 1$  when interpenetration between supra-aggregates is forced. The connectivity transition must thus be located at a  $\Phi_{mag}$  slightly higher than 0.03.

### 2.3 Homogeneity of supra-aggregates at large scale

In order to know if the supra-aggregates are homogeneously dispersed at large scale, we have taken TEM pictures of films made of nanoparticles C at rather high  $\Phi_{mag}$  ranging from 0.01 to 0.05. They are presented in Figure 6. For all the  $\Phi_{mag}$ , we observe a homogeneous dispersion of supra-aggregates with the same structural characteristics as the ones derived from the SAXS analysis of previous section. Several scans of various regions of the samples were systematically done and they show perfectly reproducible pictures over the whole TEM grid. The supra-aggregates are homogeneously dispersed in the whole PS matrix.

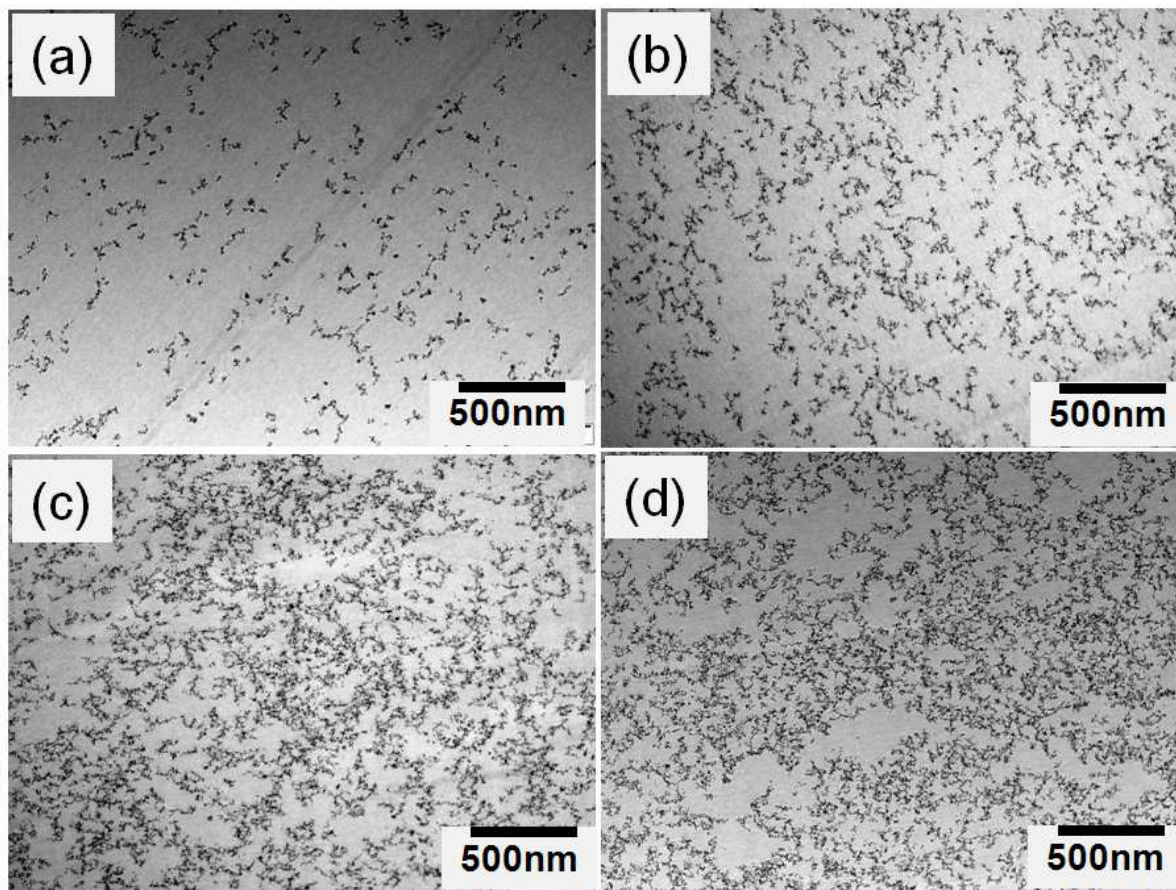


Figure 6: TEM picture of a nanocomposite made of nanoparticles C: (a)  $\Phi_{\text{mag}} = 0.01$ ; (b)  $\Phi_{\text{mag}} = 0.02$ ; (c)  $\Phi_{\text{mag}} = 0.03$ ; (d)  $\Phi_{\text{mag}} = 0.05$ .

The progressive concentration of the supra-aggregates, by increasing  $\Phi_{\text{mag}}$ , seems to lead to the percolation of the system between around  $\Phi_{\text{mag}} = 0.03$ , which is in perfect accordance with the previous SAXS analysis.

### ***3 Influence of the effect of nanoparticles size on the structure of supra-aggregates.***

We describe in this part the influence of the nanoparticles' size on the structure of the supra-aggregates. The SAXS scattering curves for the nanoparticles A, B, and D look very similar to the ones of nanoparticles C for the whole range of volume fractions. They are presented in Figure SI.3 in Supporting Information. This shows that the aggregates within the nanocomposites films are produced with a highly reproducible structure for all nanoparticles' size. There exist nevertheless some differences in the

1 structure from one size to another. We compare here the scattering of the four different batches in the  
2 three regimes of interest: (i) at  $\Phi_{\text{mag}} = 10^{-5}$  where only the primary aggregates are formed, (ii) at  $\Phi_{\text{mag}} =$   
3  $5 \cdot 10^{-4}$  where the supra-aggregates are formed, far below the percolation threshold, and (iii) at  $\Phi_{\text{mag}} =$   
4 0.03, close the percolation threshold.  
5  
6  
7  
8

9 We start first with nanocomposites polymer films diluted in nanoparticles, *i.e* where only the primary  
10 aggregates are formed. Figure 7 presents the scattering curves features for the four batches of  
11 nanoparticles. As expected, the position of the correlation peak corresponding to the contact of two  
12 nanoparticles at  $q^* = 2\pi/(2R_{\text{NP\_mean}})$  is shifted towards the low  $q$  when  $R_{\text{NP\_mean}}$  increases. However, the  
13 structure is different from one sample to another. The intensity of the correlation peak changes with the  
14 nanoparticles' size. It almost vanishes for nanoparticles D, meaning that the mean number of  
15 aggregation in the primary aggregates  $N_{\text{PA\_agg}}$  decreases when the particles size decreases. This comes  
16 from the fact that, very nicely and very surprisingly, the mean radius of the primary aggregate  $R_{\text{PA\_mean}}$  is  
17 similar for the four sizes of nanoparticles. The shape of the scattering part curves corresponding to the  
18 Guinier regime of the form factor of the primary aggregate is indeed similar for all samples, as  
19 highlighted by the guide of the eye of Figure 7 which points out the  $q$ -position where the Guinier regime  
20 starts.  $N_{\text{PA\_agg}}$  decreases from  $\sim 30$  for nanoparticles A (obtained by the same study as described in  
21 previous part) to a few nanoparticles for nanoparticles D. In this latter case, it is difficult to get  $N_{\text{PA\_agg}}$   
22 with a good accuracy because there is a large uncertainty on  $R_{\text{NP\_mean}}$ . It is due to the cross-over of the  
23 Guinier Regime of the primary aggregate with the correlation peak corresponding to the contact between  
24 two nanoparticles ( $R_{\text{PA\_mean}}$  is only almost 2 times  $R_{\text{NP\_mean}}$  for nanoparticles D). The decrease of  $N_{\text{PA\_agg}}$   
25 while increasing  $R_{\text{NP\_mean}}$  is nicely illustrated in Figure 7.b and in Figure 7.c that present TEM pictures  
26 of primary aggregates for both types of nanoparticles A and D.  
27  
28  
29  
30  
31  
32  
33  
34  
35  
36  
37  
38  
39  
40  
41  
42  
43  
44  
45  
46  
47  
48  
49  
50  
51  
52  
53  
54  
55  
56  
57  
58  
59  
60

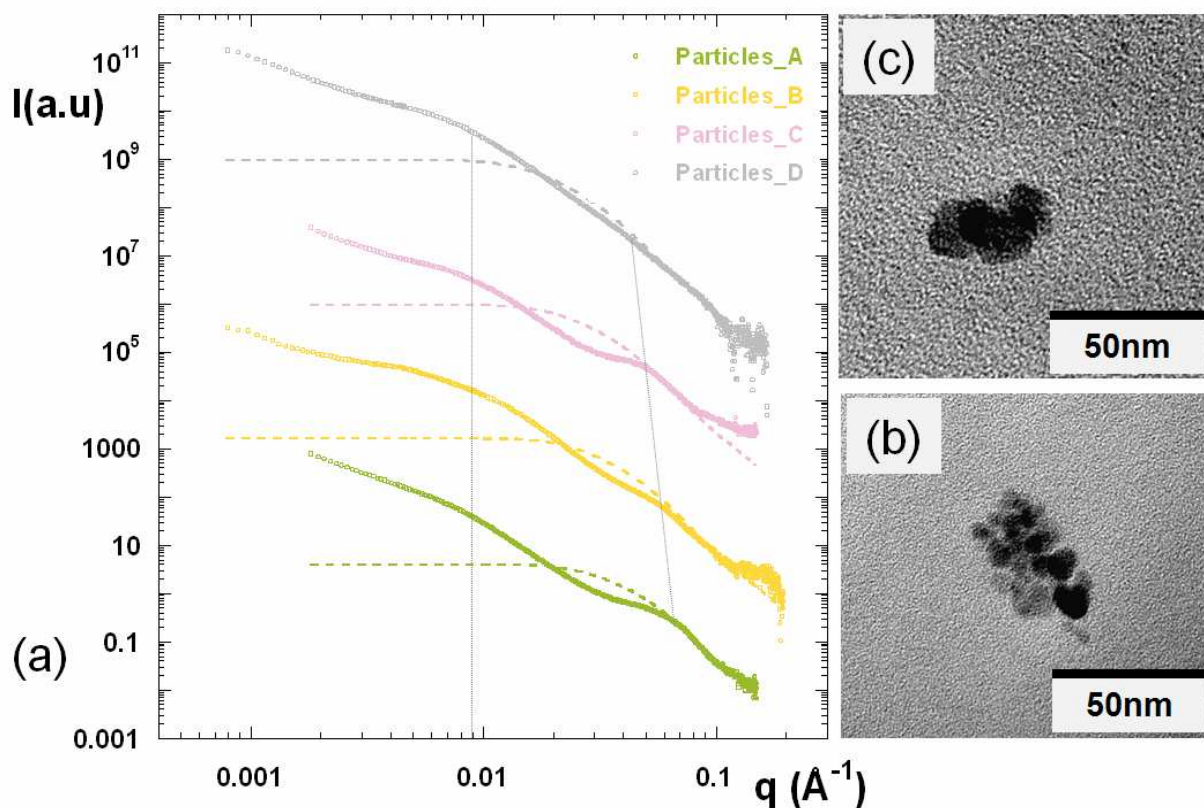


Figure 7: Influence of the nanoparticles' size on the structure of primary aggregates. (a) Comparison of SAXS spectra for the different nanoparticles batches compared with their form factor. The scattering curves are shifted in intensity for clarity. The dashed lines correspond to the form factor of the nanoparticles. The two grey lines are only guides for the eyes that point out the  $q$ -position of the Guinier regime starts and the correlation peak corresponding to the contact between two nanoparticles. (b) TEM picture of a nanocomposite made of nanoparticles A at  $\Phi_{\text{mag}} = 10^{-5}$ . (c) TEM picture of a nanocomposite made of nanoparticles D at  $\Phi_{\text{mag}} = 10^{-5}$ .

Figure 8.a presents the influence of the nanoparticles size on the structure of supra-aggregates, by comparing the SAXS scattering spectra of the four samples made at  $\Phi_{\text{mag}} = 5 \cdot 10^{-4}$ . At very low  $q$  (besides the structure of the primary aggregates), all the scattering curves are exactly the same, as highlighted Figure 8.b where all the experimental scattering curves are rescaled in intensity. Figure 8.d to Figure 8.g present TEM pictures of supra-aggregates for both types of nanoparticles A and D at  $\Phi_{\text{mag}}$

=  $5.10^{-4}$  for two different magnifications. For the 4 nanoparticles sizes, the samples form exactly the same kind of supra-aggregate made of primary aggregates of the same mean radius.

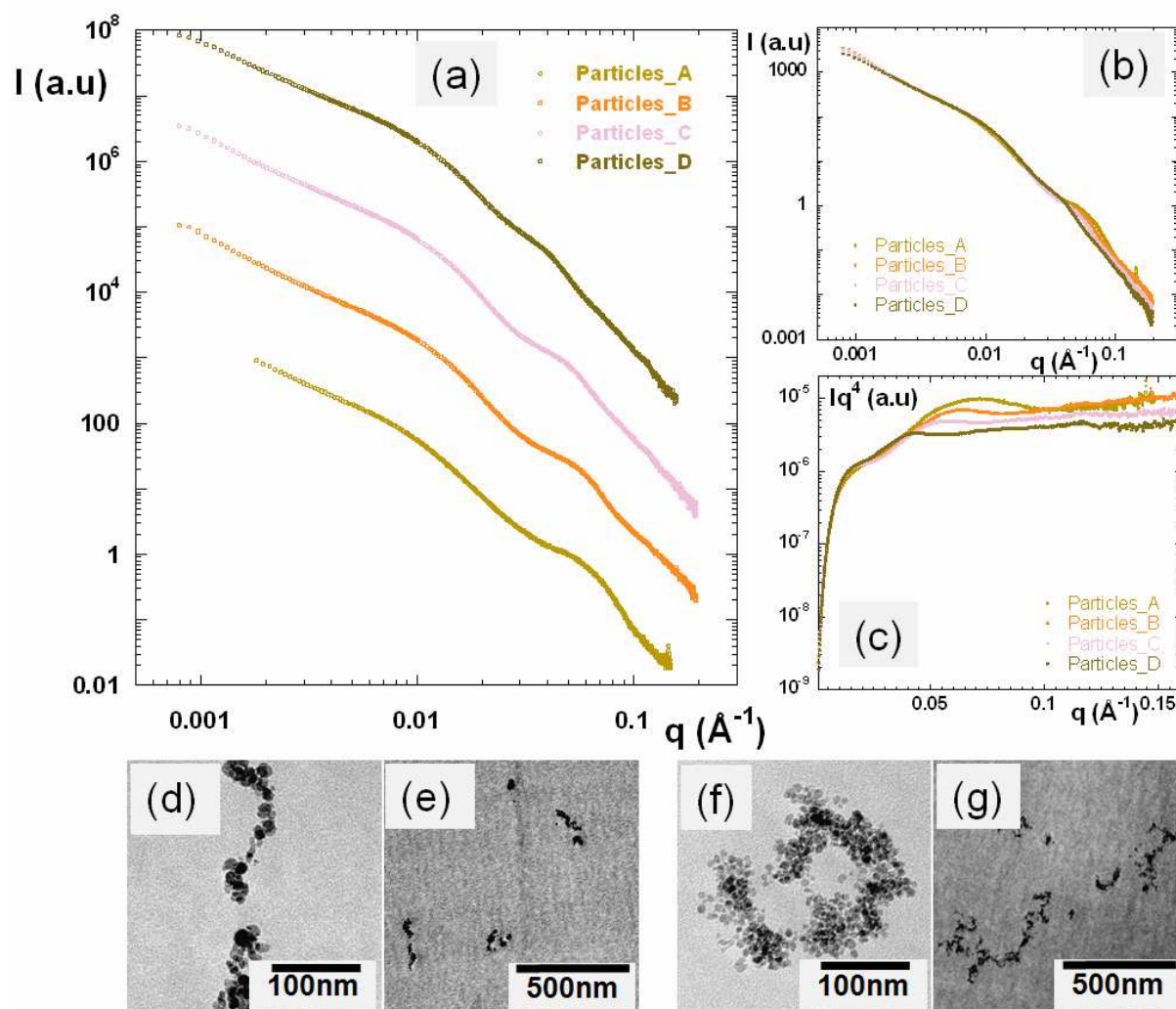


Figure 8: Influence of the nanoparticles' size on the structure of supra-aggregates. (a) Comparison of SAXS spectra for the different nanoparticles batches at  $\Phi_{\text{mag}} = 5.10^{-4}$ . The scattering curves are shifted in intensity for clarity. (b) Same scattering curves rescaled in intensity to the one of nanoparticles A. (c)  $q^4 I(q)$  versus  $q$  for the same scattering curves. (d) & (e) TEM pictures of a nanocomposite made of nanoparticles D at  $\Phi_{\text{mag}} = 5.10^{-4}$  at different magnifications. (f) & (g) TEM picture of a nanocomposite made of nanoparticles A at  $\Phi_{\text{mag}} = 5.10^{-4}$  at different magnifications.

The modification of the specific surface of the primary aggregates with the particles' size resulting from the variation of the number of the native nanoparticles per primary aggregate is illustrated in the  $I.q^4$



versus  $q$  representation of figure 8.c. At large  $q$  in the so-called limiting Porod regime, all the curves exhibit a plateau, of which intensity is directly proportional to the  $S/V$  ratio of the aggregates. This intensity nicely decreases when the nanoparticles' size increases. This means that the contact surface between the polymer matrix and the filler, i.e. the quantity of chains influenced by the proximity of the filler, can be easily tuned by the native nanoparticles' size without modifying the surface of the nanoparticles and thus the nature of the interaction with the polymer.

Figure 9 displays the SAXS scattering curves of the nanocomposites made at a higher concentration ( $\Phi_{\text{mag}} = 0.03$ ), in the regime where the supra-aggregates are close to the percolation threshold, for the four nanoparticles' size. The previous analysis is confirmed as presented in the inset of Figure 8 where all the experimental scattering curves are rescaled in intensity. They perfectly superimpose together, indicating that all the samples have the same structure in this  $q$ -range.

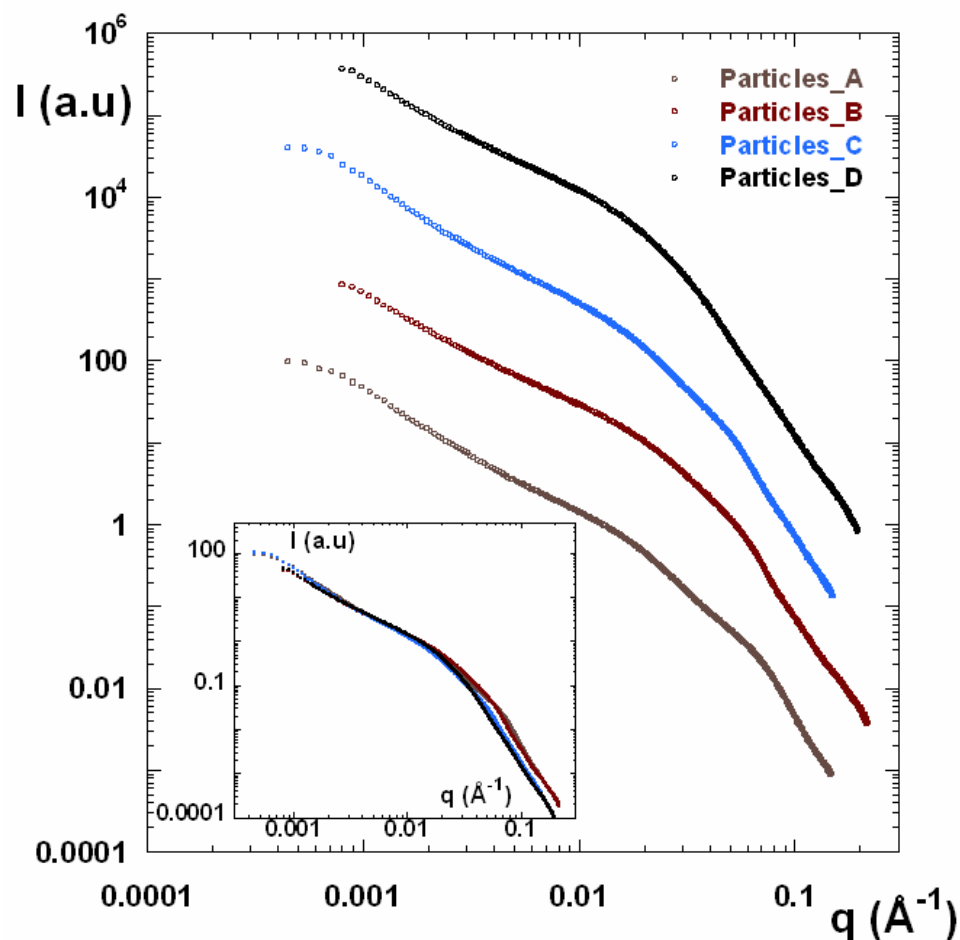


Figure 9: Influence of the nanoparticles' size on the structure of supra-aggregates. Comparison of SAXS spectra for the different nanoparticles batches at  $\Phi_{\text{mag}} = 0.03$ . The scattering curves are shifted in intensity for clarity. Inset: Same scattering curves rescaled in intensity to the one of nanoparticles A

#### 4 Mechanisms of formation of the primary aggregates and of the supra-aggregates

We discuss here about the mechanisms of formation of supra-aggregates, in spite of the fact that they remain partially poorly understood. A full understanding would require the determination of the evolution of the structure of the system at different steps during the evaporation process, which is very difficult because it is not possible to match the signal from the remaining solvent in SAXS and it is not possible to get a good statistics at very low  $\Phi_{\text{mag}}$  in SANS. However, the amount of reproducible structural data obtained here on the system allows us to reveal some major trends to describe them.

First, the aggregation of the nanoparticles occurs during the film processing, only after the beginning of the DMAc evaporation. As proven by the results of part III.2, there are still repulsions between the naked  $\gamma\text{-Fe}_2\text{O}_3$  nanoparticles when they are mixed with PS chains in DMAc. A mechanism of initial aggregation of the nanoparticles induced by the PS chains can thus be dismissed.

Second, the aggregation mechanism during drying is a two-step process. As the primary aggregates are obtained in a reproducible way for all the samples at  $\Phi_{\text{mag}}$  down to  $10^{-5}$ , they are presumably formed during an initial step of the drying. For the concentrated samples, a secondary step of aggregation, which leads to supra-aggregates, should occur only later during the drying process.

The primary aggregation step process is unexpected, and its mechanisms of formation remain unclear.

It does not come from direct interactions between nanoparticles because this aggregation step occurs even at  $\Phi_{\text{mag}}$  down to  $10^{-5}$  after drying. For  $\Phi_{\text{mag}} = 10^{-5}$ , the mean distance between two nanoparticles

$d_{\text{mean}}$  in the initial homogeneous dispersion of spheres is higher than  $(d_{\text{NP\_mean}})^3 \sqrt{\frac{\pi}{610^{-5}}}$  where  $d_{\text{NP\_mean}}$  is

1 the mean diameter of the nanoparticles. Thus  $d_{\text{mean}} > \sim 40 d_{\text{NP\_mean}}$ . For electrostatic suspensions of  
2  
3 maghemite nanoparticles of such a typical diameter, it has been shown in [Cousin 2003] that the  
4  
5 interparticle potential between nanoparticles almost vanish at  $d_{\text{mean}} \sim 3 d_{\text{NP\_mean}}$  because all the  
6  
7 interactions have a limited range (Van der Waals attractions, magnetic dipolar attractions and  
8  
9 electrostatic repulsions). Some eventual depletion interactions induced by the PS chains have also a very  
10  
11 limited range (see part III.2). Moreover, an aggregation process driven by such attractive interactions  
12  
13 would have lead to an increase of  $N_{\text{PA\_agg}}$  with  $R_{\text{NP\_mean}}$ , but the opposite effect is observed. As the  
14  
15 primary aggregation leads to clusters which always have roughly the same size, the understanding of its  
16  
17 origin may pass through the identification of the parameter of our experimental system that has such a  
18  
19 characteristic size ( $\sim 168 \text{ \AA}$ ). This is not the mean radius of the nanoparticles  $R_{\text{NP\_mean}}$ . It is much closer  
20  
21 to the gyration radius of the PS chains in  $\theta$  solvent used here (we get  $230 \text{ \AA}$  for PS chains of  $M_w$  280 000  
22  
23 g/mol). However the PS chains are in semi-dilute regime before casting with a characteristics blob size  $\xi$   
24  
25 of  $11 \text{ \AA}$  [32], a size much lower than the one of the primary aggregates. It is likely that for nanoparticles  
26  
27 of higher mean radius, the primary aggregation step would disappear.  
28  
29  
30  
31  
32

33 The secondary aggregation step process, that leads to open fractal aggregates with a  $D^f$  of 1.7, is much  
34  
35 easier to understand. This fractal dimension is indeed very close to 1.78, corresponding to the one  
36  
37 measured and computed [33] for colloids aggregated through a Diffusion Limited Aggregation (DLA)  
38  
39 process. As primary aggregates do not interact a priori, their further aggregation can thus only be driven  
40  
41 by diffusion processes. Theses processes are progressively frozen during drying, because the viscosity  
42  
43 diverges. They do not occur for very dilute systems, because the primary aggregates are too far away  
44  
45 from each other to aggregate by DLA before freezing. Once a critical concentration of primary  
46  
47 aggregates is reached (ranging from  $\Phi_{\text{mag}} = 10^{-4}$  to  $5 \cdot 10^{-4}$ ), the system becomes concentrated enough in  
48  
49 primary aggregates to allow DLA processes. The aggregation is limited at much larger scale by the  
50  
51 competing effects of both the increase of the aggregates size by the DLA and of the freezing of the  
52  
53 system, which leads to the finite size of supra-aggregates. As  $\Phi_{\text{mag}}$  has a minor impact on the viscosity  
54  
55 of the whole mixture, the process is similar for all samples, and leads to the same size.  
56  
57  
58  
59  
60

## 5 Specificity of the system

If some mechanisms of formation of the supra-aggregates remain to be understood, the clear description of the final dispersion of the maghemite nanoparticles inside the PS matrix gives an original picture. To our best knowledge, a reproducible two-step aggregation process of native nanoparticles inside a polymer matrix has never been reported in the literature on comparable systems (naked nanoparticles mixed with polymer chains). The formation of nanocomposites is usually driven by a more classical single-step aggregation process [5,34, 35] The native particles form objects of finite size at low content which percolate when increasing the concentration.

This original two-step process, associated to the possibility of tuning the polymer-filler surface contact by the size of the native particles, is a very promising way to understand the microscopic mechanisms of the mechanical properties of reinforced materials, which involve two contributions in the elastic modulus, one coming from the fillers and one coming from the polymer chain. It is actually difficult to discriminate from an experimental point of view these two contributions. Indeed, changing the polymer-filler interaction in order to probe the chain contribution usually modifies also the filler organization. Reciprocally, changing the filler structure, for example by the particles' concentration, also modifies the polymer-filler interactions.

To date, some fillers effects have been clearly described in the literature, especially the deviation of the hydrodynamic reinforcement associated to the percolation process of the fillers [Heinrich 2002]. But some other effects below the percolation threshold, like the existence of an elastic contribution, have been also observed [36]. The origin of this last contribution, which involves both the conformation [37] and the dynamic [12] of some polymer chains in the vicinity of the filler, is still under discussion. It remains indeed difficult to highlight it directly because it depends on the fraction of the implicated chains, which is difficult to evaluate and could be reduced to a small value [13]. Thus, our experimental system is of great interest to understand the contribution of the polymer chains in the mechanical

1 reinforcement because it enables to increase the fraction of the implicated chains by changing the  
2 specific surface of the fillers without changing the fillers contributions (the threshold percolation, here,  
3 is mainly related to the size of the supra-aggregates and it is independent of the size of the native  
4 maghemite nanoparticles).

## 11 **V Conclusion and perspectives**

16 We have shown here first how we have succeeded in obtaining stable colloidal suspensions of  
17 magnetic nanoparticles of maghemite ( $\gamma\text{-Fe}_2\text{O}_3$ ) of  $\sim 40 \text{ \AA}$  of radius in dimethylacetamide (DMAc), a  
18 polar solvent which is also a good solvent of several common polymer chains (PS, PMMA, ...). This  
19 was obtained by a gentle exchange of solvents by dialysis on suspensions that were initially synthesized  
20 in water, without any treatment of the bare nanoparticles. Such suspensions are promising from a  
21 polymer science point of view, as they could be the starting point of controlled polymerizations from the  
22 surface of the nanoparticles while keeping colloidal stability to achieve PS-grafted nanoparticles with  
23 controlled corona. Several successful polymerizations from different "Grafting from" routes have been  
24 reported on close systems made of silica nanoparticles stabilized in DMAc (ATRP [38], NMP [15]).

27 We have also shown that we were able to easily produce highly reproducible nanocomposites made of  
28 such  $\gamma\text{-Fe}_2\text{O}_3$  nanoparticles dispersed in a polystyrene matrix. At high volume fraction ( $\Phi_{\text{mag}} \geq 5 \cdot 10^{-4}$ ),  
29 the magnetic nanoparticles in the matrix were forming an homogeneous dispersion of supra-aggregates  
30 with a finite size of around  $\sim 200 \text{ nm}$ , with a hierarchical structure made of dense primary aggregates  
31 composed of some tens of nanoparticles. The latter supra-aggregates are organized in fractal way at  
32 higher scale with a dimension of 1.7. At low volume fraction ( $\Phi_{\text{mag}} \leq 10^{-4}$ ), only the primary aggregates  
33 were obtained. All the structural parameters of the supra-aggregates were perfectly characterized by an  
34 analysis combining SAXS and TEM microscopy.

37 A remarkable specificity of the system comes from the reproducibility of the hierarchical structure  
38 obtained at a large scale. It is indeed possible to tune the inner structure of the elementary 'bricks'

1 forming the supra-aggregates (the primary aggregates) by an appropriate choice of the initial size of the  
2 nanoparticles without altering the structure at larger scale. This provides huge potentials to the system  
3 that will be presented in forthcoming studies:  
4

5  
6  
7 (i) First, it is a perfect model system to go further in the understanding of mechanical properties of  
8 nanocomposites because it allows to uncouple perfectly the respective contribution of the filler structure and  
9 polymer dynamics to the reinforcement. It allows indeed to process different samples with the same filler  
10 structure and the same  $\Phi_{SA}$ , either below the percolation threshold or above it, but with different surface  
11 contact between the nanoparticles and the PS matrix by playing on the nanoparticles' size.  
12  
13

14  
15  
16 (ii) Second, the primary aggregates are a powerful tool to design new nanocomposites with various and  
17 controlled anisotropic morphologies of the filler, ranging from slightly anisotropic structures to highly  
18 anisotropic structures. This can be done by using an external magnetic field during casting and playing on  
19 the magnetic susceptibility of the nanoparticles, that strongly increases with the size of the  
20 nanoparticles.  
21  
22  
23  
24  
25  
26  
27  
28  
29  
30  
31  
32  
33

34 **Acknowledgements:** We thank Nicolas Jouault for fruitful discussions and for showing us how to  
35 process PS films with inorganic nanoparticles.  
36  
37  
38  
39  
40  
41

42 **Supporting Information Available.** The magnetization curves of suspensions of  $\gamma$ -Fe<sub>2</sub>O<sub>3</sub> magnetic  
43 nanoparticles in H<sub>2</sub>O, the SAXS spectra of suspensions of  $\gamma$ -Fe<sub>2</sub>O<sub>3</sub> magnetic nanoparticles in H<sub>2</sub>O and  
44 the SAXS spectra of  $\gamma$ -Fe<sub>2</sub>O<sub>3</sub> nanoparticles in the nanocomposites polymeric films are presented in  
45 Supporting Information. This material is available free of charge via the Internet at <http://pubs.acs.org>.  
46  
47  
48  
49  
50  
51  
52  
53  
54

## 55 **References**

56  
57 [1] Vaia, R. A.; Maguire, J. F. *Chem. Mater.* **2007**, *19*, 2736-2751  
58  
59  
60

- 1 [2] Tjong, S. C. *Materials Science and Engineering*, **2006**, 73-197.
- 2
- 3 [3] Guth, E.; Gold, O. *Phys. Rev.*, **1938**, 53, 322.
- 4
- 5 [4] Heinrich, G.; Kluppel, M.; Vilgis, T. A. *Current Opinion Solid State and Materials Science*, **2002**,
- 6
- 7 6, 195–203.
- 8
- 9 [5] Jouault, N.; Vallat, P.; Dalmas, F.; Said, S.; Jestin, J.; Boué, F. *Macromolecules* **2009**, 42(6), 2031–
- 10
- 11 2040.
- 12
- 13 [6] Botti, A.; Pyckout-Hintzen, W.; Richter, D.; Urban, V.; Straube, E. *J. Chem. Phys.* **2006**, 124.
- 14
- 15 [7] Kropka, J. M.; Putz, K. W.; Pryamitsyn, V.; Ganesan, V.; Green, P. F. *Macromolecules* **2007**, 40,
- 16
- 17 5424-5432.
- 18
- 19 [8] Rharbi, Y.; Cabane, B.; Vacher, A.; Joanicot, M.; Boué, F. *Europhys. Letters*, **1999**, 46, 472-478.
- 20
- 21 [9] Mark, J. E.; Abou-Hussein, R.; Sen, T. Z.; Kloczkowski, A. *Polymer*, **2005**, 46, 8894-8904
- 22
- 23 [10] Tuteja, A.; Duxbury, P. M.; Mackay, M. E. *Phys. Rev. Letters*, **2008**, 100, 077801.
- 24
- 25 [11] Nakatani, A. I.; Chen, W.; Schmidt, R. G.; Gordon, G. V.; Han, C. C. *Polymer*, **2001**, 42, 3713-
- 26
- 27 3722.
- 28
- 29 [12] Long, D.; Lequeux, F. *Europhys. Letters*, **2001**, 4, 371.
- 30
- 31 [13] N. Jouault, F. Dalmas, S. Said, E. Di-Cola, R. Schweins, J. Jestin, F. Boué, 2010, Submitted.
- 32
- 33 [14] Akcora, P.; Liu, H.; Kumar, S. K. ; Moll, J.; Li, Y.; Benicewicz, B. C. ; Schadler, L. S. ; Acehan, D.
- 34
- 35 ; Panagiotopoulos, A. Z. ; Pryamitsyn, V.; Ganesan, V.; Ilavsky, J. ; Thiyagarajan, P.; Colby, R. H. ;
- 36
- 37 Douglas, J. *Nat. Mater.*, **2009**, 8, 354-359
- 38
- 39 [15] Chevigny, C.; Gignes, D.; Bertin, D.; Jestin, J., Boué, F. *Soft Matter*, **2009**, 5(19), 3741-3753.
- 40
- 41 [16] Dalmas, F.; Cavaillé, J.-Y.; Gauthier, C. ; Chazeau, L.; Dendievel, R. *Compos. Sci. Technol.*, **2007**,
- 42
- 43 67, 829–839.
- 44
- 45 [17] Oberdisse, J.; El Harrak, A.; Carrot, G.; Jestin, J.; Boué, F. *Polymer*, **2005**, 46, 6695–6705
- 46
- 47 [18] Massart, R.; Dubois, E.; Cabuil, V. ; Hasmonay, E. *J. Magn. Magn. Mater.* **1995**, 149, 1-5.
- 48
- 49 [19] E. Dubois, E.; Perzynski, R.; Boué, F.; Cabuil, V. *Langmuir*, **2000**, 16(13), 5617-5625.
- 50
- 51 [20] Varga, Z.; Filipcsei, G.; Zrinyi, M. *Polymer*, **2006**, 47, 227.
- 52
- 53
- 54
- 55
- 56
- 57
- 58
- 59
- 60

- 1  
2  
3  
4  
5  
6  
7  
8  
9  
10  
11  
12  
13  
14  
15  
16  
17  
18  
19  
20  
21  
22  
23  
24  
25  
26  
27  
28  
29  
30  
31  
32  
33  
34  
35  
36  
37  
38  
39  
40  
41  
42  
43  
44  
45  
46  
47  
48  
49  
50  
51  
52  
53  
54  
55  
56  
57  
58  
59  
60
- [21] Galicia, A.; Cousin, F.; Cabuil, V.; Dubois, E.; Sandre, O.; Perzynski, R. *Soft Matter*, **2009**, 5, 2614-2624.
- [22] Jestin, J.; Cousin, F.; Dubois, I.; Ménager, C.; Oberdisse, J.; Schweins, R.; Boué, F. *Adv. Mater.*, **2008**, 20(13), 2533-2540.
- [23] Massart, R. *I.E.E.E. Trans. Magn.* **1981**, 17, 1247
- [24] *Magnetic Fluids and Applications Handbook*, ed. by B. Berkovski (Begell House Inc. Publ., New York, 1996.
- [25] Brûlet, A.; Lairez, D.; Lapp, A.; Cotton, J.-P. *J. Appl. Cryst.* **2007**, 40, 165–177
- [26] Cousin, F.; Cabuil, V. *J. Mol. Liq.* **1999**, 83, 203-215.
- [27] Cousin, F.; Dubois, E.; Cabuil, V. *Phys. Rev. E*, **2003**, 68(2), 021405
- [28] Israelachvili, J. *Intermolecular and Surface Forces*, Academic Press, New York, **1992**.
- [29] Scaling concepts in polymer physics
- [30] Rottler, J.; Robbins, M. O. *Phys. Rev. E*, **2003**, 68(1), 011801.
- [31] Fresnais, J.; Berret, J.-F.; Qi, L. ; Chapel, J.-P.; Castaing, J.-C.; Sandre, O.; Frka-Petesic, B.; Perzynski, R. ; Oberdisse, J.; Cousin, F. *Phys. Rev. E* **2008**, 78, 040401.
- [32] De Gennes, P.G. *Scaling Concepts in Polymer Physics*; Cornell University Press: Ithaca, NY, **1979**.
- [33] Lin, M. Y.; Lindsay, H. M.; Weitz, D. A.R.; Ball, C. ; Klein, R. ; Meakin, P. *Phys. Rev. A* **1990**, 41, 2005.
- [34] Bansal A.; Yang, H.; Li, C.; Cho, K.; Benicewicz, B. C.; Kumar, S. K.; Schadler, L. S. *Nat. Mater.* **2005**, 4, 693-698.
- [35] Sen, S. ; Xie, Y.; Bansal, A.; Yang, H.; Cho, K.; Schadler, L. S.; Kumar, S. K. *Eur. Phys. J. Spec. Top.* **2007**, 141, 161–165.
- [36] Tsagaropoulos, G.; Eisenberg, A. *Macromolecules* **1995**, 28, 6067–6077.
- [37] Sarvestani, A. S. *Eur. Polym. J.* **2008**, 44, 263–269.
- [38] Carrot, G.; El Harrak, A.; Oberdisse, J.; Jestin, J. ; Boué, F. *Soft Matter*, **2006**, 2(12), 1043-1047.



**Supporting information**

# Homogeneous Dispersion of Magnetic Nanoparticles Aggregates in a PS Nanocomposite: Highly Reproducible Hierarchical Structure tuned by the Nanoparticles' Size.

*Anne-Sophie Robbes<sup>1,2</sup>, Jacques Jestin<sup>1</sup>, Florian Meneau<sup>2</sup>, Florent Dalmas<sup>3</sup>, Olivier*

*Sandre<sup>4</sup>, Javier Perez<sup>2</sup>, François Boué<sup>1</sup>, Fabrice Cousin<sup>1,\*</sup>*

<sup>1</sup>Laboratoire Léon Brillouin, CEA Saclay 91191 Gif sur Yvette, Cedex France

<sup>2</sup>Synchrotron SOLEIL L'Orme des Merisiers, PO Box 48, Saint-Aubin, 91192 Gif sur Yvette, France

<sup>3</sup>Institut de Chimie et des Matériaux Paris-Est, CNRS UMR 7182, 2-8 rue Henri Dunant 94320 Thiais, France

<sup>4</sup>Laboratoire Physicochimie des Electrolytes, Colloïdes et Sciences Analytiques, UMR CNRS-UPMC-Univ Paris 6-ESPCI-Paris Tech 7195, 4 place Jussieu, case 51, 75005 Paris, France

\* Corresponding author: [fabrice.cousin@cea.fr](mailto:fabrice.cousin@cea.fr)

# 1 SAXS spectra of suspensions of $\gamma\text{Fe}_2\text{O}_3$ magnetic nanoparticles in $\text{H}_2\text{O}$ and DMAc

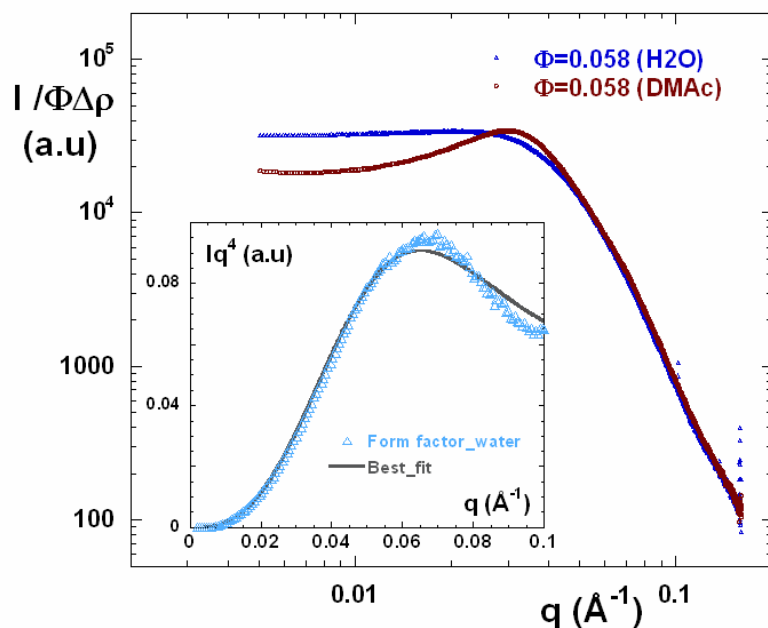


Figure SI 1.a: SAXS scattering curves for the suspensions of nanoparticles A either in water or in DMAc presented in a  $I(q)/\Phi\Delta\rho = f(q)$  representation.  $\Delta\rho$  stands either for  $(\rho_{\text{mag}} - \rho_{\text{DMAc}})^2$  or  $(\rho_{\text{mag}} - \rho_{\text{water}})^2$  depending on the solvent used. Inset:  $q^4 I(q)$  versus  $q$  for  $\Phi_{\text{mag}} = 0.001$  in water. The full line corresponds to the best fit of the form factor.

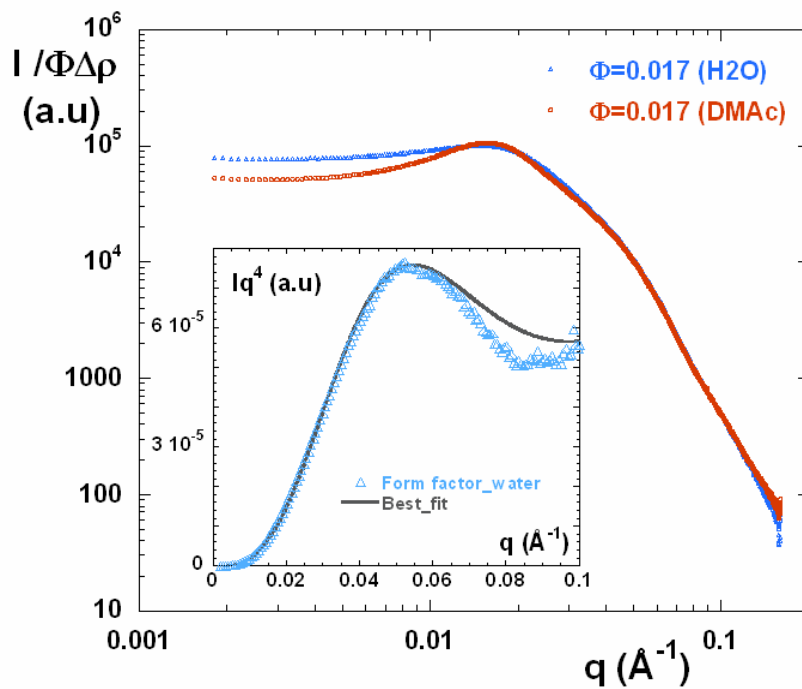


Figure SI 1.b: SAXS scattering curves for the suspensions of nanoparticles B either in water or in DMAc presented in a  $I(q)/\Phi\Delta\rho = f(q)$  representation.  $\Delta\rho$  stands either for  $(\rho_{\text{mag}} - \rho_{\text{DMAc}})^2$  or  $(\rho_{\text{mag}} - \rho_{\text{water}})^2$  depending on the solvent used. Inset:  $q^4I(q)$  versus  $q$  for  $\Phi_{\text{mag}} = 0.001$  in water. The full line corresponds to the best fit of the form factor.

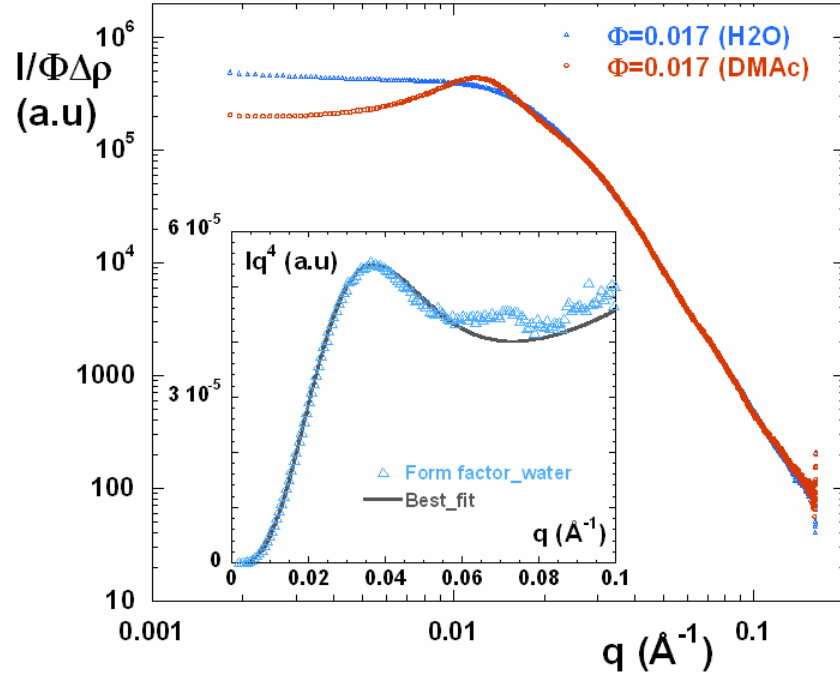


Figure SI 1.c: SAXS scattering curves for the suspensions of nanoparticles D either in water or in DMAc presented in a  $I(q)/\Phi\Delta\rho = f(q)$  representation.  $\Delta\rho$  stands either for  $(\rho_{\text{mag}} - \rho_{\text{DMAc}})^2$  or  $(\rho_{\text{mag}} - \rho_{\text{water}})^2$  depending on the solvent used. Inset:  $q^4I(q)$  versus  $q$  for  $\Phi_{\text{mag}} = 0.001$  in water. The full line corresponds to the best fit of the form factor.

## 2 Magnetization curves of suspensions of $\gamma\text{Fe}_2\text{O}_3$ magnetic nanoparticles in $\text{H}_2\text{O}$

In order to determine the volume fraction of the different suspensions after synthesis and the size distribution of the nanoparticles, we have measured the magnetization curves of the suspensions in  $\text{H}_2\text{O}$ .

We briefly recall the principle here. Each nanoparticle bears a magnetic moment  $\vec{\mu}$  which is of the order of  $10^4$  Bohr magnetons. Its modulus  $|\vec{\mu}| = m_s V_{\text{magn}}$  is proportional to the magnetic volume  $V_{\text{magn}}$  of the nanoparticles and to  $m_s$  the magnetization of the maghemite. Under a large applied field  $\vec{H}$ , this magnetic moment  $\vec{\mu}$  orientates along the field direction. In a liquid suspension of  $\gamma\text{-Fe}_2\text{O}_3$  nanoparticles of radius  $\sim 4$  nm, it also rotates mechanically the core of the nanoparticle. The alignment of  $\vec{\mu}$  along  $\vec{H}$  provides to the suspension a

macroscopic magnetization  $M$ . At saturation, all the magnetic moments align along  $\vec{H}$ , then  $M = M_S = m_s \Phi$ . For intermediate fields, the behavior of the suspension is superparamagnetic. For a suspension of monodisperse nanoparticles of radius  $R$ ,  $M$  is well described by the first Langevin law  $L(R)$  at low  $\Phi$  (when dipole-dipole correlations are neglected) :

$$M(H) = M_s \left( \coth \frac{\mu_0 \mu H}{kT} - \frac{kT}{\mu_0 \mu H} \right) \quad \text{with } M_S = m_s \Phi \quad (1)$$

For polydisperse suspensions, the shape of the curves  $M(H)$  is modified by the log-normal size distribution of the particles size  $P(R, \sigma)$  (see equation 2 of main text) :

$$\frac{M(H)}{M_s}(R_0, \sigma) = \frac{\int_0^\infty d^3 P(R) L(R, H) dR}{\int_0^\infty d^3 P(R) dR} \quad (2)$$

At low  $H$ , in the linear regime, the magnetization curve is proportional to the magnetic susceptibility of the nanoparticles. The magnetization curves are presented for the different batches of nanoparticles A, B, C and D in Figure SI.1.

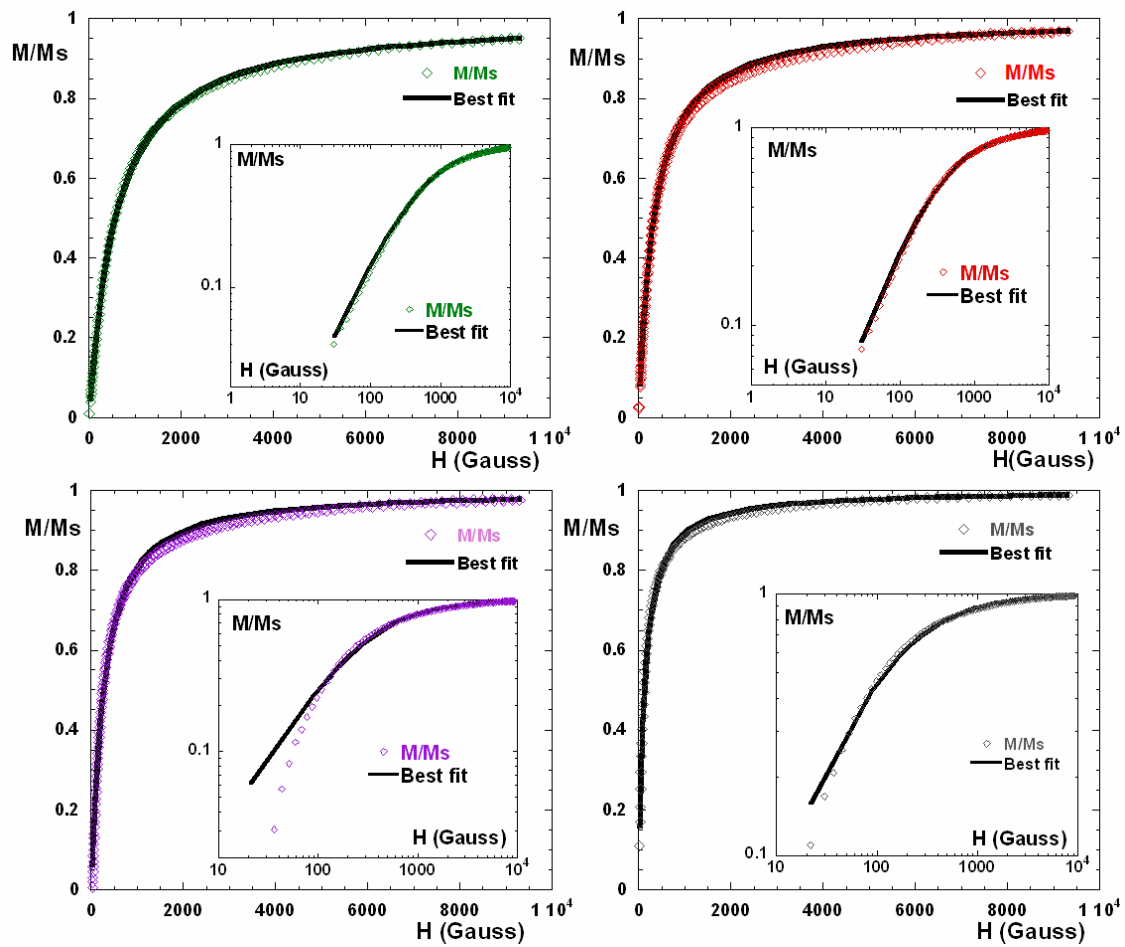


Figure SI.2: Magnetization curve of the suspensions of  $\gamma\text{Fe}_2\text{O}_3$  nanoparticles in  $\text{H}_2\text{O}$ . The magnetization curves are modelled by the first Langevin law and take into account the polydispersity of the nanoparticles. Inset: same curves in log-log scale. (a) batch A; (b) batch B; (c) batch C; (d) batch D.

### 3 SAXS spectra of $\gamma\text{Fe}_2\text{O}_3$ nanoparticles in the nanocomposite polymeric films

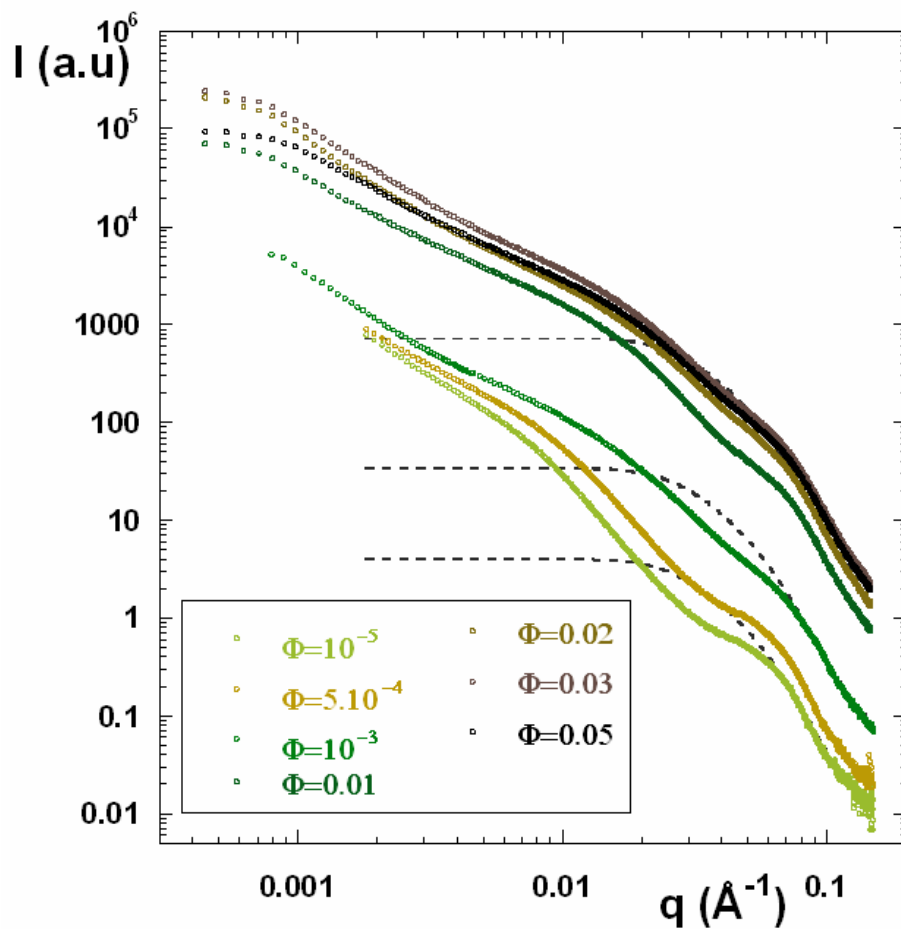


Figure SI.3.a: SAXS scattering curves of the  $\gamma\text{Fe}_2\text{O}_3$  nanoparticles in the PS polymeric matrix obtained by SAXS for nanoparticles A. The dashed lines correspond to the form factor of the nanoparticles.

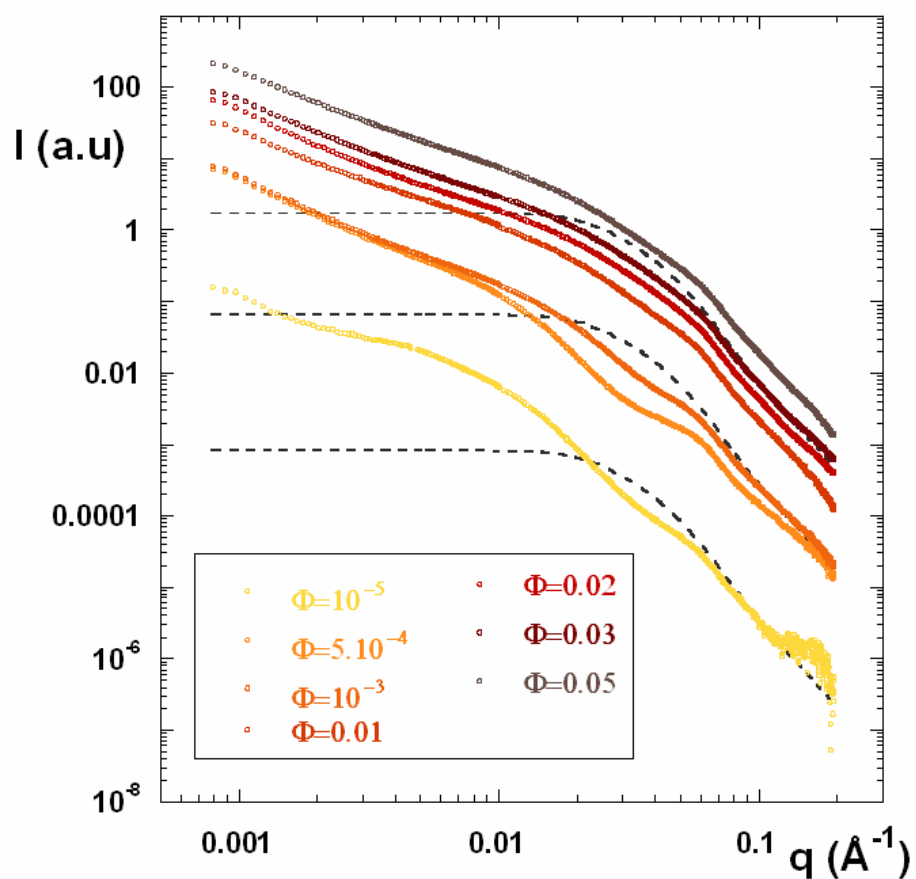


Figure SI.3.b: SAXS scattering curves of the  $\gamma\text{Fe}_2\text{O}_3$  nanoparticles in the PS polymeric matrix obtained by SAXS for nanoparticles B. The dashed lines correspond to the form factor of the nanoparticles.

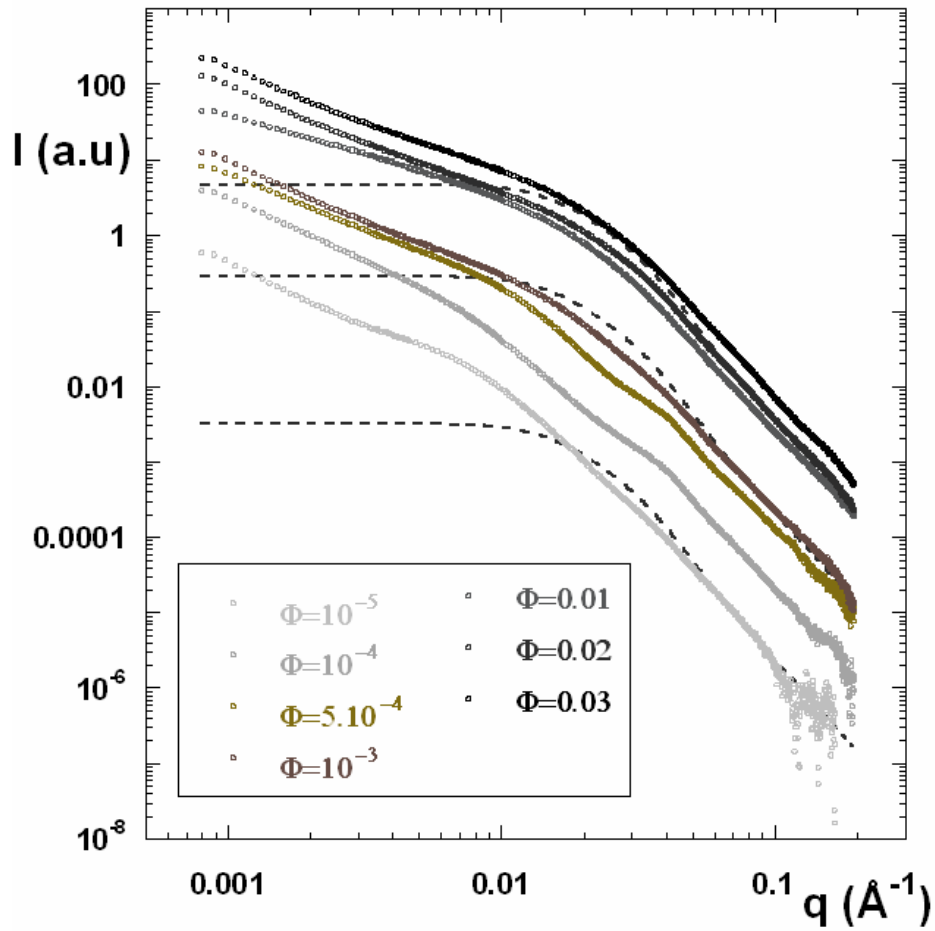


Figure SI.3.c: SAXS scattering curves of the  $\gamma\text{Fe}_2\text{O}_3$  nanoparticles in the PS polymeric matrix obtained by SAXS for nanoparticles D. The dashed lines correspond to the form factor of the nanoparticles.